Catalysis Science & Technology

Accepted Manuscript

ROYAL SOCIETY OF CHEMISTRY

www.rsc.org/catalysis

Semiconductor-Based Photocatalysts and Photoelectrochemical Cells for Solar Fuel Generation: A Review

*Jiangtian Li, Nianqiang Wu**

Department of Mechanical and Aerospace Engineering, West Virginia University, Morgantown, WV 26506-6106, USA

*To whom the correspondence should be addressed. Fax: +1-304-293-6689, E-mail: nick.wu@mail.wvu.edu

ABSTRACT

To address the challenge in sustainable global development, considerable efforts have been made to produce fuels from renewable resources with photocatalysts and photoelectrochemical cells (PECs) by harvesting solar energy. The solar energy conversion efficiency of photocatalysts and PECs is strongly dependent on the light absorption, charge separation, charge migration, charge recombination processes and (electro)catalytic activity in photoactive semiconductors. This perspective article describes the barrier, progress and future direction of research on the correlation of the chemical constituent, size, dimensionality, architecture, crystal structure, microstructure and electronic band structure of photocatalysts (or photoelectrodes) with five vital processes including light absorption, charge separation, migration and recombination as well as surface redox reactions. This article deals with both single materials and composites such as co-catalysts on photoelectrodes/photocatalysts, dye-sensitized or plasmon-enhanced photocatalysts, semiconductor-semiconductor heterostructures, semiconductor-carbon hybrids as wells as Z-scheme and tandem cells. This article also highlights the application of representative photocatalysts and PECs in solar water splitting.

Key words: photocatalyst, photoelectrochemical cell, solar fuel, water splitting, hydrogen, energy band, charge transfer, semiconductor, surface plasmon resonance

Table of Contents

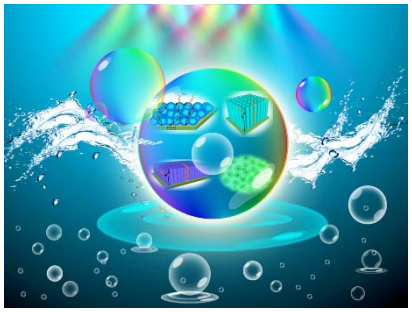

This perspective article describes the barrier, progress and future direction of research on the photocatalytic and photoelectrochemical solar fuel generation.

1. Introduction

Currently, the primary energy source is supplied from fossil fuels, which accounts for ~81% of all energy supplies in 2011 and 2012.[1,2] Combustion of fossil fuels leads to the greenhouse effect and climate change.[3-5] The environmental concern, the reducing availability of fossil fuels and the daily-increasing demand on energy supply has simulated the development of an renewable energy sources. Solar energy is a most clean, abundant renewable energy source. The energy that the sun hits the earth for one hour is much more than what human beings need for one year.[5,6] The solar energy can be converted and stored in fuels such as hydrogen by water splitting and hydrocarbon compounds by CO_2 reduction.[7-16]

In 1972, Fujishima and Honda discovered the hydrogen generation by illuminating TiO_2 electrode in a photoelectrochemical cell (PEC).[17] In 1979, the same group reported the photocatalytic CO_2 reduction by different semiconductors.[18] These two discoveries have opened a new avenue for solar fuel production. The US Department of Energy (DOE) has set up a target for PEC hydrogen production to achieve the solar-to-hydrogen (STH) efficiency of 10% with durability of 5000 hours till 2018.[19,20] DOE also targets to reach $5.7/gge (gasoline gallon equivalent) for photoelectrode systems and $4.6/gge for photo-particle systems in 2020. Although efficiencies as high as 12.4% for a tandem cell and 18% for a multijunction cell have been achieved, high cost and long-term instability of the employed semiconductors hindered their commercialization.[21-23] It is recognized that the technology for solar water splitting is still far from maturity, and the current R&D priority is put on the material and device development.

Photocatalysts and photoelectrochemical cells have been reviewed in the previous papers.[9-16] This perspective article will place an emphasis on the correlation of the photocatalytic/photoelectrochemical performance of semiconductors with materials features and the five vital physico-chemical processes including (i) light absorption, (ii) charge separation, (iii) charge migration, (iv) charge recombination and (v) surface redox reactions. The material features such as the chemical constituent, size, dimensionality, architecture, crystal structure, microstructure and electronic band structure govern these five physico-chemical processes, which in turn determine the solar energy conversion efficiency of semiconductor-based photocatalysts and PECs.[24-27] In the present work, we attempt to provide insight into the physico-chemical processes. We also review the technical barriers in development of photocatalyst/photoelectrode materials. We will then discuss the strategy for designing new

materials and structures for photocatalysts/photoelectrodes.

2. Photocatalysis and Photoelectrochemical Cells

2.1 Concepts and Testing of Photocatalysts and Photoelectrochemical Cells

The detailed introduction to photocatalysis refers to previous excellent papers.[24,25] Briefly, semiconductor photocatalysis drives a heterogeneous photochemical catalytic reaction on the surface of a solid-state semiconductor.[28] There are two basic configurations for photocatalytic generation of fuels: the particulate system and the PEC as shown in Figure 1. In a particulate system, the free-standing photocatalyst powders are either suspended in a solution or fixed at a reactor bed. As shown in Figure 1, five main processes occur: (I) light absorption, (II) charge separation, (III) charge migration, (IV) charge recombination and (V) redox reactions.[24-27] When a semiconductor absorbs the photons with the energy greater than the band gap energy (E_g), electrons are excited to the conduction band, leaving the holes in the valence band. The separated electrons and holes then migrate through the semiconductor to the semiconductor/electrolyte interface, where redox reactions occur to generate fuels. However, not all the photo-generated charge carriers can be collected and finally contribute to the fuel generation. In fact, a portion of the photo-generated charge carriers are subject to the recombination in the bulk and at the surface, dissipating their energy thermally by creation of phonons and so on.[29] Charge recombination is believed to be a major loss of the excited charge carriers and a critical factor that limits the solar-to-chemical energy conversion efficiency for semiconductor photocatalysts. The charge carriers have a recombination time on the order of 10^{-9} s while the chemical interaction with adsorbed species has a longer time scale between 10^{-8}-10^{-3} s.[30] Studies show that the charge recombination can sometimes reach up to 90% within a period of 10 ns after generation.[4,31]

The amount of produced hydrogen and oxygen can be quantitatively measured by gas chromatograph. The fuel production rate is typically evaluated by the amount of fuel per unit time. The apparent quantum yield (*QE*) is typically used to evaluate the performance of photocatalysts as follows[32]

$$QE = \frac{2 \times number\ \ of\ \ H_2\ \ molecules}{number\ \ of\ \ incident\ \ photons} \qquad (1)$$

$$QE = \frac{4 \times number\ of\ O_2\ molecules}{number\ of\ incident\ photons} \qquad (2)$$

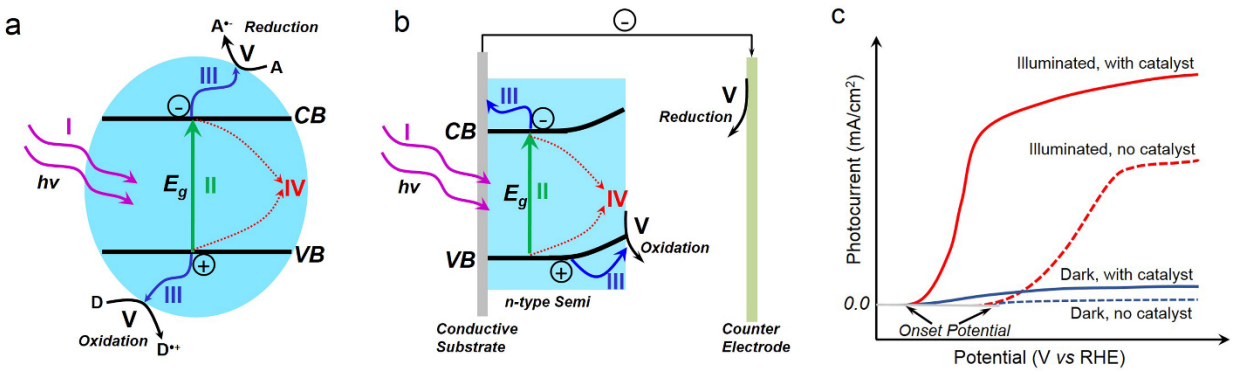

Figure 1. Scheme illustration of (a) a particulate photocatalyst, (b) a photoelectrochemical (PEC) cell with a n-type photoelectrode, (c) Photocurrent density-voltage curves obtained from a *n*-type semiconductor photoanode. Note: (I) Light absorption, (II) Charge separation, (III) Charge migration, (IV) Charge recombination and (V) redox reaction. CB=Conduction band, VB=Valence band, E_g=Band gap, A=Acceptor, and D=Donor.

In a PEC, the photoelectrode is made of semiconductor, which is supported on a conductive substrate as the working electrode (a *n*-type semiconductor as the anode and a *p*-type semiconductor as the cathode). Different from the particulate system, the reduction and oxidization reactions occur on the different electrodes separately. For example, in a PEC with an n-type semiconductor photoanode for overall water splitting, hydrogen is generated at the cathode while oxygen is evolved at the photoanode surface. Thus the reaction products can be collected in separate chambers. The PEC configuration provides great flexibility in designing materials. The photoactive and catalytic materials can be applied on the separate electrodes that are located in different chambers. Also, in a PEC, the Fermi level of the photoelectrode can be controlled via a potentiostat; and the redox reactions can be controlled at a desirable potential so that reaction selectivity can be improved. Moreover, a PEC is a powerful tool for studying the photo-induced charge separation and charge transfer processes in semiconductors as well as the reaction kinetics and mechanism at the semiconductor/electrolyte interface.

In order to make comparative evaluation, an effort has been made to publish the standard methods for testing the performance of PECs. [33] A photocurrent density-voltage (J-V) curve is an important tool used for testing PECs (Figure 1c), in which a primary performance indicator for a PEC is the photocurrent density (mA/cm^2) at an applied voltage of 1.23 V (*vs.* RHE, the reversible hydrogen electrode) for a photoanode and at 0 V (*vs*. RHE) for a photocathode, respectively. Alternatively, the solar-to-chemical energy conversion efficiency (η) can be quantitatively measured for a two-electrode PEC, which requires an external bias to drive a redox reaction, as follows [33]

$$\eta = \frac{J(V_{redox} - V_{app})}{P_{light}} \quad (3)$$

where J is the measured photocurrent density (mA/cm^2), V_{redox} is the redox potential of a reaction. V_{redox} =1.23 V for electrochemical water splitting. V_{app} is the applied external bias (V). P_{light} is the measured intensity of the full-spectrum solar radiation (mW/cm^2). In addition, the quantum efficiency of a two-electrode PEC is typically quantified by the incident photon-to-electron conversion efficiency (*IPCE*), which is calculated as [33]

$$IPCE = \frac{1240 \cdot J}{\lambda \cdot P_{\lambda}} \quad (4)$$

where λ is the wavelength of the incident light (nm), and P_{λ} is the measured irradiance at the specific wavelength (mW/cm^2). In addition, the transient photocurrent is typically acquired to study the long-time scale charge recombination behavior in a semiconductor photoelectrode.[34] Also, electrochemical impedance spectroscopy (EIS) is an important tool that is able to gain in-depth understanding of physic-chemical processes in a PEC. For example, the space charge capacitance (C_{SC}) near the semiconductor surface in an electrolyte can be derived from EIS. The relationship of the donor density (N_D) in a semiconductor photoelectrode with C_{SC} can be obtained via the Mott-Schottky equation [33]

$$\frac{1}{C_{sc}^2} = \frac{2}{\varepsilon_o \varepsilon_r e N_D A^2}(V_{app} - V_{fb} - \frac{kT}{e}) \quad (5)$$

where ε_o is the vacuum permittivity, ε_r is the relative permittivity, A is the photoelectrode area, V_{fb} is the flat band potential, k is Boltzmann constant and T is temperature. From the plot of

$1/C_{sc}^2$ vs. V_{app} (called Mott-Schottky plot), N_D and V_{fb} can be obtained. Also, the Mott-Schottky plot can tell whether the semiconductor is a p-type or n-type. The above-mentioned photoelectrochemical test methods have been extensively used in the previous papers. [35,49,228,259]

2.2 Requirements of Materials for Photocatalysts and Photoelectrodes

One of important applications of photocatalysts or PECs is solar water splitting for hydrogen and oxygen generation.[4-15] The materials used for photocatalysts/photoelectrodes must enable the light absorption, the charge separation, migration and transfer to the electrolyte solution for redox reactions. This leads to high demand on the semiconductor as follows.

Wide light absorption spectral range: As shown in Figure 2, the theoretical maximum solar-to-hydrogen (STH) efficiency is determined by the band gap of semiconductors. The semiconductor should have a small band gap to absorb the sunlight in a wide spectra range to achieve high a STH efficiency.

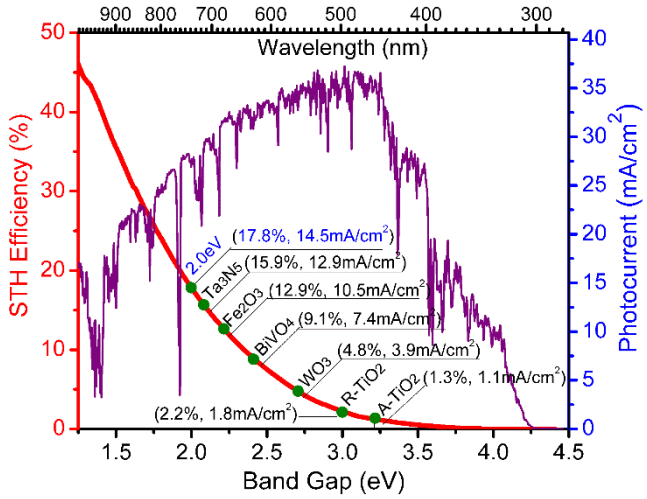

Figure 2. Dependence of the theoretical maximum solar-to-hydrogen (STH) efficiency and the photocurrent density of photoelectrodes on the band gap under AM 1.5 G irradiation (100 mW/cm^2).

Suitable band energetics: The conduction band (CB) and the valence band (VB) levels must straddle the redox potentials of the photocatalytic reaction.[3,10-14] Taking water splitting as example

$$H_2O \leftrightarrow H_2 + \tfrac{1}{2}O_2 \qquad (6)$$

Water splitting is a thermodynamically uphill reaction, which requires the Gibbs free energy of 237.18 kJ·mol^{-1}. In view of the electrochemical potential, a minimum potential of 1.23 V is required at 293 K.[36,37] Therefore, the minimum band gap of the semiconductor for water splitting should be 1.23 V plus the required overpotentials. Meanwhile, the conduction band position must be more negative than the H_2 generation potential, and the valence band more positive than the O_2 generation potential to promise the overall water splitting. Figure 3 summarizes the band edge positions of some widely studied semiconductors.[10,38] The dashed lines indicate the water redox potentials.

High charge mobility and long charge carrier diffusion length: The charge recombination is responsible for a major loss of the solar energy conversion efficiency. High charge mobility and long charge carrier diffusion length are demanded to ensure a low charge recombination rate.

Strong catalytic activity: The photoanode and photocathode should have good catalytic activity toward water oxidation and reduction, respectively, to reduce the overpotential.

Good stability: The semiconductor must chemically, electrochemically and photoelectrochemically stable in the electrolyte.

Sustainability and low cost: The last but not the least, to meet the global sustainable development, the materials employed should be inexpensive, earth-abundant, environmentally friendly, and are desirable to be synthesized via "green" processes.

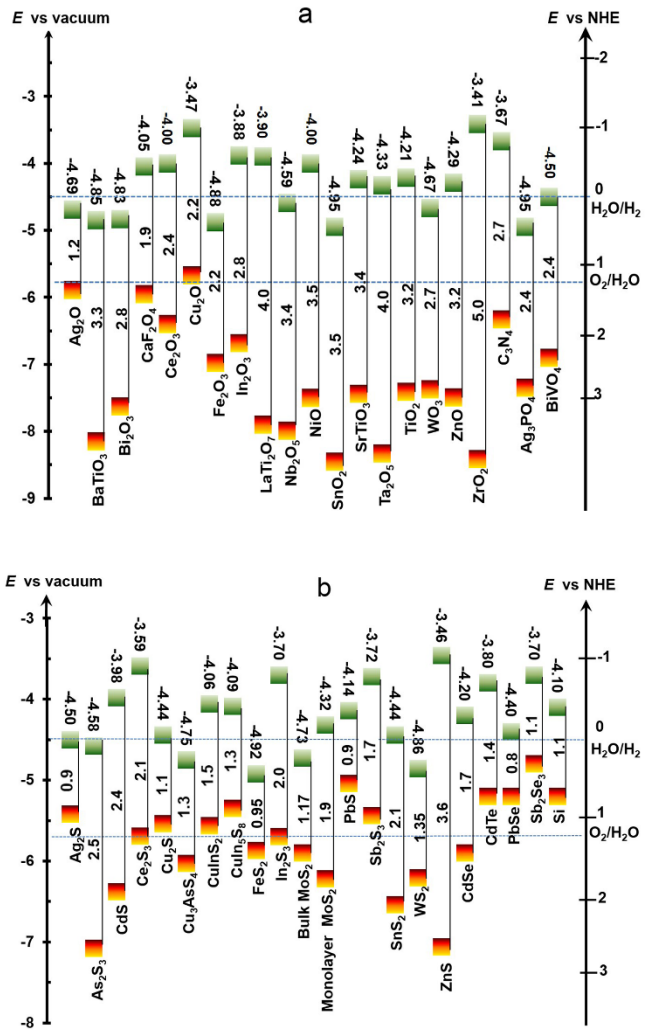

Figure 3. Band edge positions with respect to the vacuum level and the NHE for selected semiconductors at pH 0. The top squares represent the conduction band edges; the bottom squares present the valence band edges. The top numbers show the exact conduction band level and the number between squares is the band gap. The two dashed lines indicate the water redox reaction potentials. The data are adopted from Ref. 38 with the permission from the Mineralogical Society of America, and modified with new literature. [10, 13, 30, 52]

3. Single materials

3.1 Highlights of Typical Materials for Photocatalysts and Photoelectrodes

Since 1972, researchers have selected or developed many semiconductors for photocatalysts/photoelectrodes, such as metal oxides, metal chalcogenides, metal nitrides, carbon nitrides and III-V compounds. Several representative photoactive semiconductors are highlighted

here.

TiO_2: It is the first materials used for photoelectrochemical water splitting and still serves as the benchmark for photocatalyst/photoelectrode materials. It has a wide band gap (3.2 eV for anatase 3.0 eV rutile phase) and an optical penetration depth of δ_p=250 nm at λ=308 nm of incident light,[39] where δ_p is the depth at which the intensity of incident light is decayed to *1/e* of original value. The minority (hole) diffusion length (L_D) is 70 nm for anatase TiO_2 [40] and 10 nm for rutile phase.[41] TiO_2 is earth abundant, non-toxic and photochemically stable under harsh condition. However, owing to its large band gap, it can only absorb the ultraviolet (UV) light, which accounts for <5% of solar radiation. This leads to a very low theoretical maximum STH efficiency (η=1.3% for anatase and 2.2% for rutile TiO_2). In the last decade, many attempts were made to dope TiO_2 with either anions or cations to enable the visible-light photocatalytic activity. Although doping can extend its light absorption spectral range from the UV light to the visible light, the optical absorbance is low in the visible-light region. In addition, the doped TiO_2 typically exhibit a low photocatalytic activity in the visible-light region and may harm on the UV photocatalytic activity.

Fe_2O_3: It is earth abundance, non-toxicity, stable, and has an optical penetration depth of δ_p=118 nm at λ=550 nm.[42] It has an ideal band gap (1.9-2.2 eV),[43] thus can achieve a theoretical maximum STH of 12.9%, which exceeds the STH benchmark efficiency of 10% for practical application.[44] However, its actual efficiency is hindered by its very short minority (hole) diffusion length (2-4 nm), low minority charge carrier mobility and poor water oxidation kinetics, which causes the accumulation of most photogenerated holes near the surface, leading to high surface and bulk charge recombination rates.[45-47] To overcome these shortcomings, nanostructures are commonly employed to enable the holes to migrate to the surface.[45-49] The water oxidation kinetics can be improved using co-catalysts. Deposition of IrO_2 on hematite surface has led to a photocurrent of 3.3 mA/cm^{-2} at 1.23 V (vs. RHE), shifted the on-set potential by 200 mV.[48] The world-record photocurrent for hematite (4.32 mA/cm^{-2} at 1.23 V *vs*. RHE) was achieved recently using cobalt-phosphate (Co-Pi) co-catalyst on highly crystalline worm-like hematite photoanode.[50]

$BiVO_4$ (BVO): It has an optical penetration depth of δ_p=100-500 nm at λ=420-530 nm [51] and a direct band gap of 2.4 eV with conduction band at near 0 V (vs. RHE).[52-55] It is thermodynamically favorable for the water oxidation half reaction, but requires an externally

applied bias for water reduction half reaction. The theoretical maximum STH efficiency is 9.1% and the theoretical maximum photocurrent is 7.4 mA/cm^2.[44,52,56] However, so far the theoretical maximum STH efficiency cannot be achieved due to serious charge recombination and low water oxidation kinetics. BVO has a majority (electron) diffusion length of only ~10 nm, and minority (hole) diffusion length of ~100-200 nm.[55,57,58] This causes excessive consumption of electrons by charge recombination. Doping BVO with Mo and W can significantly increase its electron diffusion length to ~300 nm with a diffusion coefficient of 1.5×10^{-7}cm^{2}s^{-1}.[44,55-60] As the water oxidation half reaction is a four-proton transfer process, the poor kinetics for O_2 evolution at the BVO surface constrains its efficiency. Therefore, it is necessary to load the co-catalysts on BVO for oxygen evolution reaction (OER). Co-Pi is the most commonly used co-catalyst for the water oxidation kinetics.[57-60] A large cathodic shift up to ~440 mV and almost complete elimination of the surface charge recombination losses have been achieved with Co-Pi as the co-catalyst for W-doped $BiVO_4$.[57] The highest photocurrent was claimed to be 2.73 mA/cm^2 at 0.6 V (*vs*. RHE) on the nanoporous $BiVO_4$ photoanode with a FeOOH/NiOOH dual-layer as the OER catalyst.[61]

CdS: It has an optical penetration depth of δ_p=62 nm at λ=500 nm[62] but a long charge carriers diffusion length up to the micrometer scale.[63-66] CdS has a band gap of 2.4 eV with the conduction band and the valence band that straddle the redox potentials for water splitting.[10,67] Thus CdS theoretically is suitable for the overall water splitting under the visible light irradiation. However, its low water oxidation kinetics leads to the accumulation of photogenerated holes, leading to photocorrosion.[10,67] Therefore, hole-scavenger sacrificial agents such as sulfide or sulfites, which have much faster oxidation kinetics than that of water oxidation, is used to protect CdS from photocorrosion. In addition, its hydrogen evolution reaction (HER) rate is extremely low for CdS alone due to the presence of a large amount of surface defects that trap the photogenerated electrons, which requires to employ the co-catalysts for HER such as Pt, Pd, PdS and MoS_2.[68-74] On the other hand, recent study shows that a low hole transfer rate was an efficiency-limiting factor in a CdS-based heterostructure.[75]

III-V compounds: The III-V compound semiconductors, such as GaAs, InP, GaP and their ternary and quaternary alloys are attractive for solar water splitting.[67,76] First, the III-V semiconductors have the desirable band gaps for light absorption (*e.g.*, 1.42 eV for GaAs 1.35 eV for InP and 2.26 eV for GaP).[77] Their band gap can be tailored by alloying (*e.g.*, 1.83 eV for

$InGaP_2$, 0.36-1.42 eV for $In_xGa_{1-x}As$ depending on the In/Ga ratio).[78,79] Second, they exhibit extraordinary charge carrier mobility (Figure 4).[76] At 300 K, GaAs has an electron mobility up to 9200 $cm^2V^{-1}S^{-1}$, and its hole mobility up to 400 $cm^2V^{-1}S^{-1}$. Surface recombination, however, is a critical factor that limits its efficiency.[80,81] Multi-junction has been considered as an efficient way to address this issue.[82-84] Multijunction PEC devices based on III-V semiconductors have demonstrated the impressive STH efficiency exceeding 16%.[82,83] However, the instability and high-cost put a constraint on these III-V semiconductor devices.[79,84]

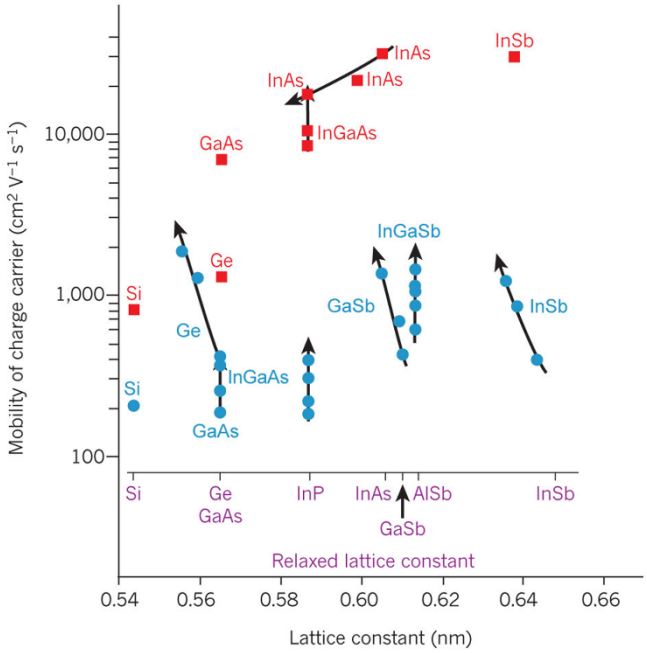

Figure 4. Electron (red) and hole (blue) mobility of III-V compounds. Reprinted from Ref. 76 with permission from Nature Publishing Group.

3.2 Size of Nanostructures

In the last decade, research on nanostructured photocatalytic and photoelectrochemical systems increased dramatically. The performance of semiconductor is strongly correlated with its size. Herein the size of nanostructure refers to the diameter, the transverse dimension and the thickness for zero-dimensional (0D), one-dimensional (1D) and two-dimensional (2D) materials, respectively. When the size of materials falls into the nanoscale, materials may exhibit the different properties.

As the size is reduced down into the nanometer scale, the percentage of atoms or ions exposed on the surface massively increases, leading to an increase in the surface-to-volume ratio. This increases the number of active sites for catalytic reactions. Therefore, nanoscale materials may also exhibit high surface activity that does not exist in the bulk.[85,86] For example, molybdenum disulfide (MoS_2) is a nontoxic, environmentally friendly and earth-abundant semiconductor with a potential to replace precious metal catalysts for hydrogen evolution reaction (HER). Bulk MoS_2 has poor catalytic activity toward HER[87] while nano-sized or monolayer MoS_2 is very active for HER[88]. Therefore, both the size and the surface effects are of great importance to photocatalysis.

As a consequence of the size reduction, a cascade of electronic properties of material also changes dramatically. Particularly, as the size of a semiconductor is smaller than its Bohr radius, the movement of the charge carriers is greatly confined in a physical size due to the quantum confinement effect, which results in the discrete electronic band structure, leading to size-dependent electronic and optical properties.[89,90] Size and band gap are inversely related in semiconductor crystals such as quantum dots (QDs). As a result, some unworkable surface reactions become prospective by controlling the semiconductor to a suitable size. [10,89,90] For example, bulk MoS_2 is an indirect semiconductor with a band gap of around 1.1 eV, which does not meet the requirement of band edge energetics for solar water splitting. When bulk MoS_2 is engineered to monolayers, a MoS_2 monolayer becomes a direct semiconductor with a band gap of around 1.9 eV [91,92], which provides the thermodynamic drive force for both photocatalytic water oxidation and reduction. Therefore, 2D MoS_2 monolayers are desirable for photocatalytic HER compared to the bulk counterpart.

Size is an important factor when considering the light absorption of semiconductors. The optical absorption in a semiconductor can be considered to follow the Beer-Lambert Law ($I_d = I_o e^{-\alpha d}$), depending on the wavelength-dependent absorption coefficient (α) [93]. The optical penetration depth (δ_p) is defined as $\delta_p = 1/\alpha$. For example, δ_p is 118 nm at a wavelength of 550 nm for Fe_2O_3 [94]. At the depth of $3\delta_p$=354 nm, the intensity of incident light is about 5%. In other words, 95% of incident light is absorbed within a thickness of 354 nm. Therefore, the optimal thickness of a thin film photoelectrode should be about $3\delta_p$ in view of light absorption.

Size is also a critical factor when considering the charge recombination. For a thin film photoelectrode, the optimal thickness is around L_D+W, where L_D and W are the minority

diffusion length and the depletion layer width, respectively. And $L_D = \sqrt{D_m \tau_m}$, where D_m is the minority diffusion coefficient and τ_m is the minority carrier lifetime.[93] This indicates that all the charge carriers photo-generated within a distance (L_D+W) away from the photoelectrode/electrolyte interface could migrate to the photoelectrode surface. The charge carriers beyond this distance are subject to recombination. For example, the minority (hole) diffusion length is 2-4 nm for the Fe_2O_3 photoanode.[48,49] Taking a depletion layer width of 7 nm, the Fe_2O_3 film photoanode should be around 9-11 nm thick. This concept has been demonstrated by the nanoscale cauliflower-shaped hematite photoelectrode [95], which offers a few hundreds of nanometers for the optical path but only a few nanometers for the minority charge carrier (hole) transport path. This nanostructured photoanode has exhibited a photocurrent density of 2.3 mA/cm^2 at 1.23 V (*vs*. RHE) in the absence of a co-catalyst on the hematite surface.

For nanostructured semiconductors, although the charge recombination inside a material is reduced as the size is reduced, the surface and interfacial charge recombination may increase considerably with an increase in the specific surface area.[96] Surface modification is demonstrated to help reduce these losses.[97-99] For example, deposition of anatase TiO_2 onto the rutile TiO_2 nanorod can effectively reduce the charge carrier traps on the surface. [100]

3.3 Dimensionality and Architecture

Semiconductors with different dimensionalities (0D, 1D, 2D and 3D) have been explored as photocatalysts/photoelectrodes as shown in Figure 5. Free-standing 0D nanoparticles are typically used as photocatalysts. In a suspension of nanoparticles, light scatters at both the front and the back sides of the nanoparticles, increasing the effective optical path length (Figure 5a). In addition, the suspended nanoparticles are isolated from each other, the nanoscale in all three dimensions promises the short charge carrier diffusion pathways. However, if nanoparticles are assembled into a photoelectrode configuration (Figure 5a), the photogenerated electrons have to transfer through inter-particle pathways to reach the charge collector. In this process, thermally activated hopping and electron tunneling occur at the inter-particle boundary, which increases the chances for charge recombination and back reactions.[86] Although a porous photoelectrode made of nanoparticles has a large specific surface area, the charge transport in such a photoelectrode is characteristic of slow diffusion via the multiple trapping and de-trapping events in the boundaries of nanoparticles. [101-103]

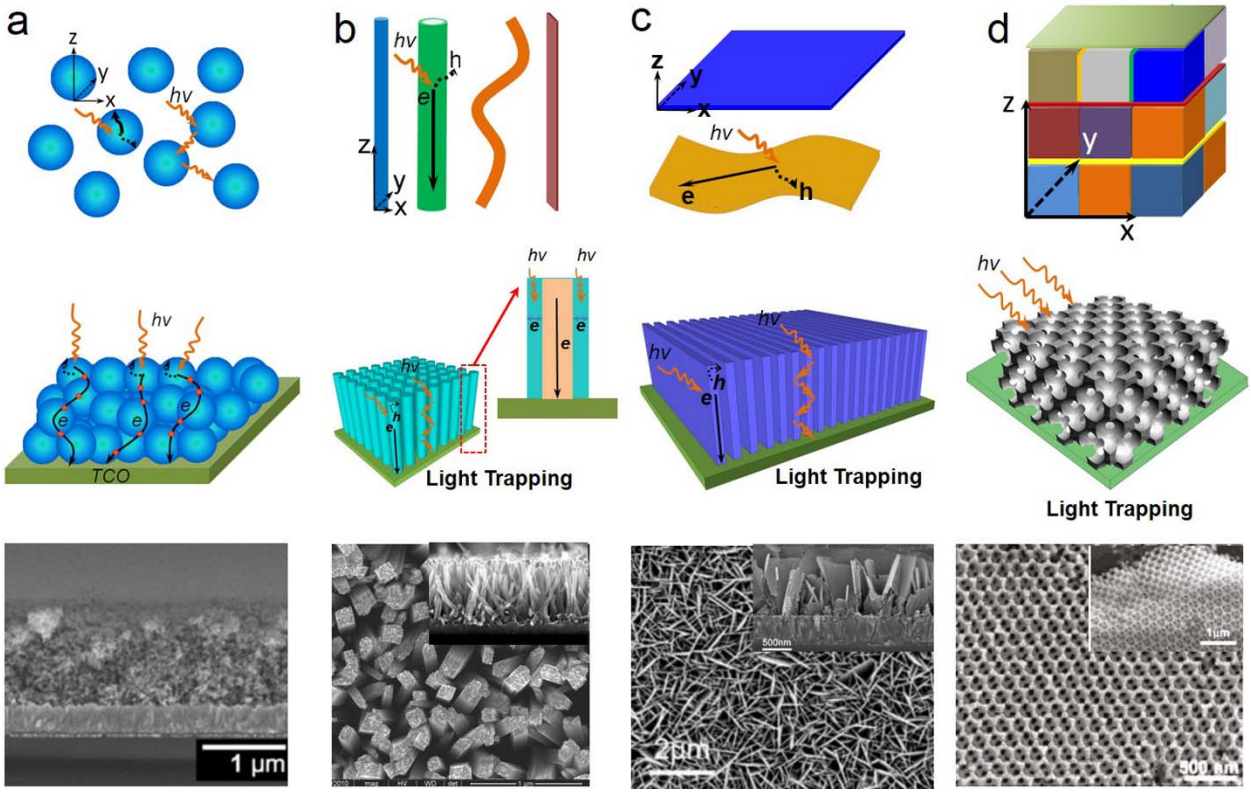

Figure 5. Light scattering/trapping and charge transport in nanoscale architectures for single material as the photoelectrode or the suspension photocatalyst. (a) 0D nanocrystals, (b) 1D nanostructures, (c) 2D nanosheets and films, and (d) 3D nanostructures constructed with 0D, 1D and 2D building block units. Adapted from Ref. 104 with permission from John Wiley. The corresponding SEM images present (*a*) TiO_2 nanoparticles, (*b*) TiO_2 nanorod array, (*c*) TiO_2 nanosheet array, and (*d*) WO_3 porous photonic crystals constructed photoelectrodes, respectively. Reprinted from Ref. 105-108 with permissions from the PCCP Owner Societies, Royal Society of Chemistry and American Chemical Society.

Different from 0D nanoparticles, 1D nanomaterials possess one dimension from the nanoscale to the micrometer scale and even longer. Nanowires, nanorods, nanotubes, nanofibers and nanobelts are typical representatives for this kind of architecture (Figure 5b). The enlarged length provides a "highway" for the charge transport along the longitudinal direction in a 1D single-crystalline nanomaterial.[109] The charge separation in 0D nanoparticles is not as effective as that in bulk because of the confined space in the nanostructure.[110] This can be alleviated in 1D nanostructures where the charge carriers are less localized compared to 0D nanoparticles.[109,111] For this reason, 1D nanostructured semiconductors are of particular interest

in solar energy conversion devices. A comparative study by Nick Wu's group has demonstrated that the single-crystalline TiO_2 nanobelts with two dominant surfaces of (101) facet exhibited better photocatalytic activity than the 0D nanosphere counterparts (Figure 6).[109] The nanobelts yielded an enhanced reactivity with O_2 molecules on the (101) facet, which produced more superoxide anions by trapping the photogenerated electrons, facilitating the charge separation. In addition, compared to 0D nanosphere counterparts, the TiO_2 (101) nanobelts exhibited a lower charge recombination rate due to greater charge mobility, fewer localized states near the band edges and in the band gap and enhanced reactivity with O_2 molecules on the (101) facet.

Another advantage of 1D nanomaterials is the light trapping and scattering, where light gets reflected between nanowires (Figure 5), dramatically increasing the path length of incident light, which is different from the large outward reflection as seen in a planar electrode.[112,113] The enhancement of light path length is dependent on the geometry of 1D nanostructures.[114] Leaky mode resonances could occur with either proper nanowire inter-spacing or diameter, which increases the light absorption. As such, it could be possible to control the light absorption enhancement at a desired wavelength by tuning the nanowire diameter.[115]

A vertically aligned 1D nanostructure array on a transparent conductive substrate is of particular interest to a photoelectrode (Figure 5b). [100,116] For a 2D thin film photoanode, the direction of light absorption is the same as the direction of charge carrier transport. In many cases (e.g. Fe_2O_3), the minority diffusion length of photoactive semiconductor is much shorter than the optical penetration depth. The maximum thickness of a 2D thin film photoanode is determined by the minority diffusion length. A vertically aligned core-shell nanorod array, in which the core and the shell are made of a highly conductive material and a photoactive material, respectively, can solve this problem because this kind of nanorod array can separate the directions of light absorption from the charge transport. [11,117] The incident light travels along the longitudinal direction of nanorods while the charge carriers migrate through the shell thickness along the transverse direction (Fig.5b). This architecture is of particular interest to the photo-active semiconductors such as Fe_2O_3 with its minority diffusion length much shorter than the optical penetration length. For example, Dunwei Wang's group has demonstrated a $TiSi_2$-Fe_2O_3 core-shell nanonet array as the photoanode for solar water splitting, in which a highly conductive metallic $TiSi_2$ nanonet acted as the charge transport channel while a 25 nm thick Fe_2O_3 shell served as the photoactive material.[118] This core-shell nanonet increased the photocurrent density

from about 0.3 to 1.6 mA/cm^2 at 1.23 V (*vs*. RHE).

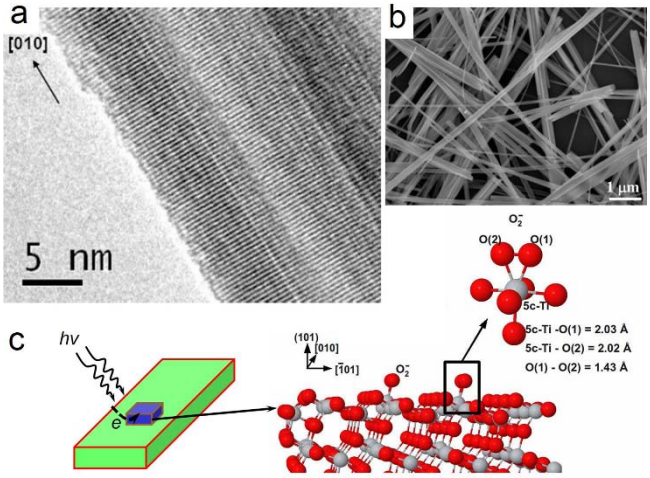

Figure 6. Anatase TiO_2 with exposed (101) facets. (a) HRTEM and (b) SEM images of TiO_2 nanobelts. (c) Geometry of anatase (101) TiO_2. Reprinted from Ref. 109 with permission from American Chemical Society.

2D nanomaterials refer to materials with two dimensions out of nanoscale range, such as free-standing nanosheets or planar films deposited on a substrate as shown in Fig. 5c. In most cases, the free-standing nanosheets as photocatalysts work as similar to 1D nanostructures. Compared to 1D nanostructures, the two large-area dominant surfaces of 2D single-crystalline nanosheets can be engineered to a highly reactive facet for photocatalysis. Moreover, the nanosheets with high specific surface area act as the physical support to form composites with other catalysts. The large face-to-face contact between nanosheets facilitates the formation of the heterojunction and interfacial charge transfer.[103] More details of 2D photocatalysts can refer to the previous paper.[103]

3D materials can be constructed by assembly of 0D, 1D or 2D nanomaterials as building blocks in a precise and ordered arrangement.[119] Assembly can be guided under a template (such as a self-assembled polymer spheres and block co-polymers) or by the inherent force of the nanoscale blocks into a 3D ordered structure. 3D ordered structures possess desired properties that cannot be achieved with disordered or suspended building blocks. For example, some 3D nanostructures have unique optical features, e.g., waveguiding, light trapping and scattering. Semiconductor photonic crystals, as one of representatives as shown in Fig. 5d, can create a photonic band gap. The light that enters the photonic crystal undergoes strong coherent multiple

scattering and propagates with a very low group velocity near the photonic band edges, which is referred as slow-light effect, which can considerably increase the effective optical path length.[108,120] It was observed that the light absorption can be enhanced orders of magnitude.[121] To maximize the light absorption enhancement, slow-light propagation modes in the inverse opal photonic crystal should be designed to be resonant with a light frequency around its electronic absorption edge.[122] Photonic-crystal-based optical coupling offers a new strategy to modify the intrinsic optical interactions inside a material. [108,123,124]

3.4 Crystal Structure and Microstructure

Crystal structure determines the electronic band structure and physico-chemical properties of semiconductors.[125] For instance, TiO_2 has four types of crystal structures: anatase, rutile, brookite, and TiO_2(B).[85] Anatase and rutile TiO_2 are commonly used as photocatalysts with band gaps of 3.20 eV and 3.0 eV, respectively. Although rutile TiO_2 can capture more light due to a narrower band gap, it exhibits lower photocatalytic activity than anatase TiO_2. Both of them are composed of TiO_6 octahedra with each Ti^{4+} ions surrounded by six O^{2-} ions. But rutile octahedra share two edges while anatase octahedra share four edges.[4,25,85] This makes longer Ti-Ti distance and shorter Ti-O distance with lower symmetry in anatase TiO_2. Anatase TiO_2 has advantages over rutile phase in terms of the charge dynamics.[126] First, it has better charge carrier mobility and longer charge carrier lifetime.[127] Second, it exhibits larger depletion layer width and stronger band bending.[128,129] As a result, surface hole trapping dominates the spatial charge separation in anatase due to the strong upward band bending. In rutile, bulk recombination of electrons and holes prevails since only the holes very close to surface can migrate to the surface.[127,130] Anatase TiO_2 exhibits a charge recombination rate about ten times lower than rutile.[4] Third, anatase has a conduction band level higher by 0.2 eV, providing higher driving force for the water reduction reaction.

It is worth noting that a mixture of anatase and rutile TiO_2 phases (*e.g.*, Degussa P25 with an anatase/rutile ratio 70/30) typically displays much higher photoactivity than any single phase TiO_2. At the anatase/rutile interface, the space charge layer is built, leading to band bending. As a result, the electric field at the interface promotes the charge separation and suppresses the charge recombination.[100,106,126,131,132] It is postulated that photo-generated electrons can transfer from anatase to rutile, and the holes can transfer in an opposite direction.[133,134]

Both single- and poly-crystalline materials have been used for photocatalysts/photoelectrodes. Single-crystalline materials have better charge mobility and lower charge recombination rate compared to polycrystalline counterparts. In polycrystalline materials, grain boundaries impede the charge transport and act as the sites for charge recombination. [135-137]

One of advantages of single crystals is their capability of selectively exposing the crystal facets on the surface. The photocatalytic activity can be tuned by tailoring the exposed crystal facets. Different facets have different surface energies. For rutile TiO_2, the {111} facet has a relatively high surface energy.[138] For anatase TiO_2, the crystal facet is ranked in terms of surface energy as γ{110} (1.09 $J \cdot m^{-2}$) > γ{001} (0.9 $J \cdot m^{-2}$) > γ{100} and {010} (0.53 $J \cdot m^{-2}$) > γ{101} (0.44 $J \cdot m^{-2}$).[139] The crystal facet with a high surface energy is active in photocatalysis. Anatase TiO_2{001} has exhibited better photocatalytic activity than other facets except for {110}.[140] Preparation of most active anatase TiO_2{110} is still a challenge. For Ag_3PO_4, the crystal facet is ranked in terms of surface energy as {111}>{110}>{100}.[141,142] It has been reported that the exposed {111} facet in Ag_3PO_4 promoted the photo-generation of electron-hole pairs and suppressed the charge recombination because of the dispersion between the valence band and the conduction band. [141]

When the exposed facets with different surface energies co-exist in a single entity, the offset of the band energy levels between different facets facilitates the charge transfer and thus enhances the photocatalytic activity.[143] In addition, studies have shown that different crystal facets are preferable for either photoreduction or photooxidation. For instance, the rutile {011} facet serve as the metal oxidation sites while the {110} facet offers the metal reduction sites.[144,145]

It remains a significant challenge to synthesize the single crystals with the desirable exposed facets because the surface facet with a high surfaced energy usually is thermodynamically unstable, thus diminishes rapidly due to minimization of surface energy during the growth process. Special surfactants that passivate the highly active facets are usually employed to guide the crystal growth. For example, for exposure of {001} facets in anatase TiO_2, fluorides are employed to control the exposure percentage.[140,146]

3.5 Electronic Band Structure and Doping

The electronic band structure governs many properties of a semiconductors, which controls the light absorption, the charge separation, migration and recombination as well as the thermodynamic drive force for photocatalytic chemical reactions.[24,85,147] This in turn has significant influence on the photocatalytic/photoelectrochemical performance of semiconductors.

The electronic band structure determines the nature of optical transition.[93] For direct semiconductors, the optical transition does not require a change in the crystal momentum, they can absorb all the incident light within a few of micrometers. As a result, the charge carriers in direct semiconductors migrate in a relatively short distance to reach the electrolyte. In contrast, indirect semiconductors require a change in the crystal momentum during optical transition. Since incident light (photon) possesses little momentum, indirect transition requires the involvement of phonons (lattice vibration). As a result, indirect semiconductors need much larger thickness (typically a few hundreds of microns) to absorb the incident light completely. Consequently, the charge carriers deep in an indirect semiconductor with a short minority charge diffusion length may be recombined before they reach the electrolyte. The absorption coefficient ($\alpha(E)$) above band gap (E_g) is expressed by $\alpha(E) = \alpha_0\sqrt{\frac{E-E_g}{E_g}}$ for a direct semiconductor, and $\alpha(E) = \alpha_0(\frac{E-E_g}{E_g})^2$ for an indirect semiconductor. The photon energy is given by $E=h\nu=hc/\lambda$, where c is the light velocity in vacuum and λ is the wavelength of light. When plotting $\alpha(E)$ versus E, the indirect semiconductors typically exhibit the Urbach tail.

In addition, the electronic band structure affects the charge carrier mobility, which is dependent on the widths of the conduction and the valence bands. The charge carrier mobility is inversely proportional to the effective mass of the carriers (either electrons or holes) that is determined by the curvature of individual bands.[93] Broad bands are largely curved, leading to small effective mass and high charge carrier mobility.

Also, the electronic band structure is correlated to photo-corrosion of semiconductors during solar fuel generation.[148] Generally speaking, smaller band gap leads to more vulnerability to photo-corrosion. Although some narrow band gap semiconductors such as Si, Cu_2O, CdSe, $CuInSe_2$ and GaAs have an advantage of wide light absorption spectral range, they are subject to photo-corrosion when acting as the photoelectrodes during solar water splitting. Generally, in view of thermodynamics, if the energy level of anodic decomposition ($E_{p,d}$) is lower with respect to the valence band edge of a semiconductor, anodic decomposition of

semiconductor will not take place. If the energy level of cathodic decomposition ($E_{n,d}$) is higher with respect to the conduction band edge, cathodic decomposition will not happen.[10,149] However, this thermodynamic rule cannot be simply used to judge the photocorrosion of semiconductors. Taking TiO_2 as an example, $E_{p,d}$ is higher than the valence band, which implies the possibility of anodic photocorrosion. In fact, anodic photocorrosion does not occur in TiO_2 due to the extremely slow reaction kinetics. Photocorrosion of semiconductors can be inhibited by addition of a suitable sacrificial agent to the electrolyte. Alternatively it can be alleviated by deposition of a suitable co-catalyst on the surface of semiconductor.

Moreover, the electronic band structure has an influence on the thermodynamic potentials for photoelectrochemical reactions. For example, the energy band edge positions of semiconductors must straddle the energy levels of water reduction and oxidation in order to photoelectrochemically split water. Shifting up the conduction band edge with respect to the water reduction level increases the thermodynamic drive force for water reduction.

Furthermore, the electronic band structure determines the spectral range of light absorption of semiconductor and the theoretical maximum solar-to-hydrogen (STH) efficiency as shown in Figure 2.[44,56,79] For example, the theoretical maximum STH efficiency is only 0.22% for $SrTiO_3$ (E_g=3.7 eV) and 1.3% for anatase TiO_2 (E_g=3.2 eV). The most effective approach to increase the conversion efficiency is to reduce the band gap to extend the light absorption spectral range into visible-light region (~43% of total solar radiation) and even near-infrared light region (~80% of total solar radiation).[36,44] However, the band gap must be large enough to meet the thermodynamics and kinetics requirements for water splitting. In viewpoint of thermodynamics, the minimum energy is required to overcome the standard Gibbs free energy change (1.23 eV) for water splitting plus the thermodynamic losses (0.3-0.5 eV). [150,151] In viewpoint of kinetics, an overpotential of 0.4-0.6 eV is required to enable a fast reaction.[23] Therefore, an ideal band gap is 1.9-2.3 eV for solar water splitting. TiO_2 is a benchmark semiconductor for photocatalysis but it has a wide band gap (3.2 eV for anatase). Hence it can only absorb the UV light, which is less than 5% of total solar radiation.[85]

As described above, the electronic band structure is the key to solar water splitting. Hence researchers have been persistently finding a solution to engineer the electronic band structure. Doping is one of common routes to extend the light absorption of wide band gap semiconductors to the longer wavelength region. Asashi *et al.* first reported the visible-light absorption of TiO_2

by N doping in 2001.[152] Since then, TiO_2 has been extensively doped either at the Ti sites with transition metal cations such as Cu, Co, Ni, Cr, Fe, and Mn.[153-155] or at the O sites and/or interstitial sites with non-metal anions such as N, C, S, P and B.[27,156-161] Generally, doping leads to the extension of light absorption spectral range. However, it may or may not bring great benefit to photocatalytic activity, which depends on the doping-induced change in the electronic band structure.

In the first case, doping does not change the band gap, but it introduces the shallow- or deep-level states[162], as shown in Figure 7(b). Both the shallow- and deep-level states are able to extend the light absorption spectral range to the longer wavelengths. Compared to the pristine semiconductor (Figure 7(a)), a doped semiconductor shows an add-on shoulder on the edge of absorbance curve (Figure 7(b)). [162] And the optical absorption cross-section of these defects is quite small. Although the mid-gap deep-level states can extend the light absorption spectral range of wide band gap semiconductors from the UV light to the visible-light range, they make little or no contribution to the visible-light photocatalytic activity because the charge carrier mobility in these states is very low[163] and these states act as the charge recombination centers [162,164]. The shallow-level states could improve the charge carrier mobility and increase the minority carrier diffusion length.[165,166] For example, doping Fe_2O_3 with Ti greatly improves the conductivity.[49,167] However, the shallow-level state may still serve as the charge recombination centers. [154,162,168] Nick Wu's group recently found that nitrogen-doping did not alter the band gap of TiO_2. Instead, it induced the localized N 2*p* state above the valence band and the 3*d* states of Ti^{3+} below the conduction band.[162] Both the localized states made limited contributed to the visible-light absorption. It is interesting that N-doped TiO_2 has improved the visible-light photocatalytic activity a little but reduced the UV-light photocatalytic activity. These two energy levels affected the photocatalytic activity differently. The gap between the N 2*p* levels and the conduction band was smaller the band gap of TiO_2, leading to the visible-light photocatalytic activity. The oxygen vacancies and the associated Ti^{3+} species reduced the photocatalytic activity by acting as the recombination centers, which consumed the photo-generated charge carriers.

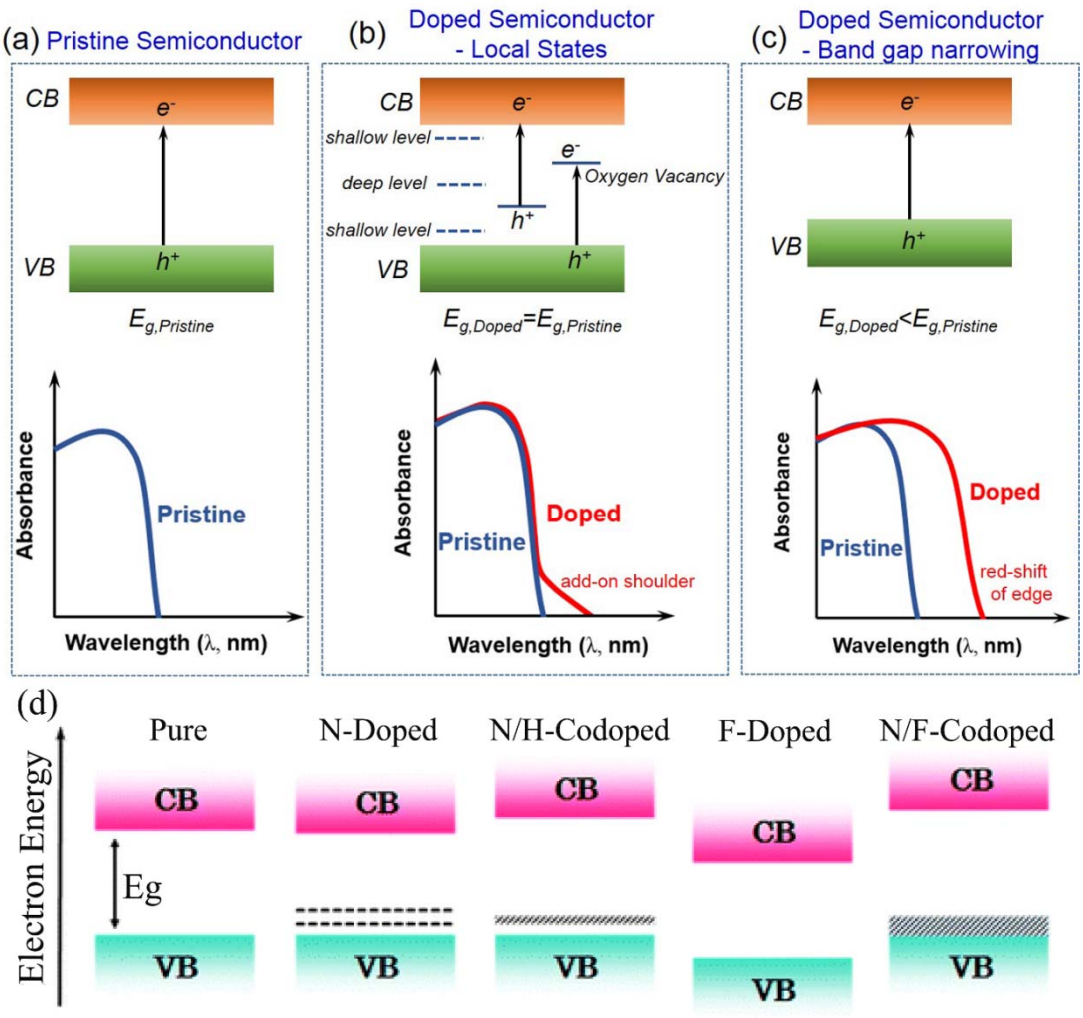

Figure 7. Scheme for engineering the electronic band structure of semiconductors. The band structure and optical absorption curves of (a) a pristine semiconductor, (b) doping-induced shallow-level and deep-level states and (c) doping-induced band gap narrowing. (d) Change in the band structure of $AgTaO_3$ resulting from different dopants; Reprinted from Ref. 178 with permissions from the PCCP Owner Societies and Royal Society of Chemistry.

Recently hydrogenated TiO_2, also called black TiO_2, has received intense attention as the visible-light photocatalyst for water splitting. Mao *et al.* first reported the synthesis of black TiO_2 by hydrogenation at 20 bar H_2 atmosphere for 5 days,[169] which initiated the enormous studies on this material since then.[170-177] It is interesting that hydrogenation-induced visible-light absorption is not main cause of its improved photocatalytic activity because the improvement mainly occurs in the UV-light region.[169-171] Two main models were proposed to explain the

visible and near-infrared light absorption in black TiO_2: (i) surface disorder and (ii) oxygen vacancy. Surface disorder-engineering by hydrogenation was proposed to destroy the lattice periodicity and to generate two tails from the VB and CB to narrow the band gap. [169] Another reason is the formation of the oxygen vacancies. Li *et al.* found that the hydrogenation of rutile TiO_2 did not shift the valence band; and they assumed that the colorization of TiO_2 was originated from the presence of oxygen vacancies.[171] However, the oxygen vacancies in many cases have proven to jeopardize the photocatalytic activity as the recombination center. So far, the underlying mechanism of the better UV-light photoactivity and the limited visible-light photoactivity of hydrogenated TiO_2 remains ambiguous.

In another case, doping into a semiconductor leads to the narrowing of band gap without introduction of any local states inside the band gap, which brings benefit to both the light absorption and the photocatalytic activity.[179] Recently Nick Wu's group observed this phenomenon in the nitrogen-doped $La_2Ti_2O_7$.[179] Compared to pristine $La_2Ti_2O_7$, N-doped $La_2Ti_2O_7$ showed a parallel shift of the whole optical absorption edge to the longer wavelength direction, as shown in Figure 7(c). The XPS analysis revealed that N-doping in $La_2Ti_2O_7$ led to the upshift of the valence band and the narrowing of the band gap. This strategy not only increases the light absorption in the visible-light region but also improve the photocatalytic activity in the UV-light region. As a result, the N-doped $La_2Ti_2O_7$ showed much better photocatalytic activity toward hydrogen generation than the pristine counterpart. [180]

A recent study has demonstrated that the electronic band gap can be engineered by doping. [178] Figure 7(d) shows that N-doping into $AgTaO_3$ led to the discrete local states above the valence band while N/H co-doping can delocalize the discrete shallow-levels. In contrast, F-doping induced the narrowing of band gap by down-shifting the conduction band while N/F co-doping resulted in the narrowing of band gap by broadening the valence band. As a result, N/F co-doping extended the light absorption spectral range, maintained the necessary drive force for water reduction, enhanced the charge separation, increased the hole mobility in the valence band, and prevented from the presence of mid-gap local states.

An alternative approach to modulate the valence band of a semiconductor is to form a solid solution. It has been demonstrated that *p-d* repulsion for III-VI semiconductors leads to a shift of the valence band maximum upward while retaining the conduction band unchanged.[181] For example, both ZnO and GaN have a large band gaps over 3 eV, however, their solid solution can

absorb light up to 500 nm.[182,183] It was believed that *p-d* repulsion in the solid solution causes an upshift of the valence band, leading to the narrowing of band gap.[184] Similar band gap narrowing was also observed in other solid solutions such as $AgAl_{1-x}Ga_xO_2$,[185] $Ca_{1-x}Bi_xV_xMo_{1-x}O_4$[186] and $(AgNbO_3)_{1-x}(SrTiO_3)_x$.[187] Solid solution offers a promising way to improve the visible-light photocatalytic activity of semiconductors because it does not introduce the localized states between the VB and the CB.

4. Composite Materials

As mentioned above, no single material can achieve 10% of STH efficiency so far. To improve the STH efficiency, two or more materials have been combined together to form a composite, which can utilize the strengths of individual materials and compensate their shortcomings and even create new functionality.

4.1 Plasmonic Metal-Semiconductor Composite photocatalysts/Photoelectrodes

As described in Section 3.5, the optimal band gap of single materials is 1.9~2.3 eV. This indicates that the sunlight with a wavelength longer than 653 nm cannot be harvested by the PEC if a single semiconductor is used as the photoelectrode/photocatalyst for solar water splitting. Incorporation of a semiconductor with a plasmonic metal nanostructure is an alternative solution to this problem. In a metal nanostructure, surface plasmon resonance (SPR) is established when the frequency of incident light matches the frequency of excited conduction electrons at the interface between metal and a dielectric.[188] SPR can be categorized into two forms: (i) surface plasmon polariton (SPP) propagating at the metal/dielectric interface, and (ii) localized SPR (LSPR) with non-propagating, collective oscillation of the surface electrons in metal nanostructures.[189-191] It has been reported that incorporating plasmonic nanostructures with semiconductors increases the efficiency of photovoltaic cells and the photocatalytic activity of semiconductors toward water splitting or organic compound decomposition.[188-192] SPR enhances the photocatalytic activity of semiconductors in three pathways: [189] (i) an increase in the light absorption by photonic enhancement,[193] (ii) enhancement of the charge separation in the semiconductor via either the direct electron transfer (DET)[194,195] or the plasmon-induced resonance energy transfer (PIRET) process, [196] and (iii) reduction of the charge recombination rate by the plasmon-mediated electromagnetic field. [193]

Photonic enhancement: Plasmonic metal nanostructures can increase the light absorption of semiconductors in three ways as shown in Figure 8a.[190] Large particles at the interface between two dielectrics can guide the incident light preferentially into the dielectric with the larger permittivity.[197] Light trapping thus occurs by scattering forward and backward in the semiconductor multiple times to effectively increase the optical path length. Although small plasmonic metal nanoparticles lead to weak light scattering, the nanoparticles embedded in the semiconductor film can create a strong local electromagnetic field with intensity up to ~10^3 times the incident field, which increases the light absorption cross-section remarkably.[188] For a periodic metal nanostructure on the back surface of the semiconductor layer, SPP mode can guide the incident light along the lateral direction and efficiently trap the light in the semiconductor.[190, 198] All three ways refer to photonic enhancement, which contributes to enhancement in light absorption and charge separation at the energies above the band gap of semiconductor.[189] The photonic enhancement strategy is suitable for thin film semiconductors with a small absorption coefficient, such as Si and hematite.[190,199,200]

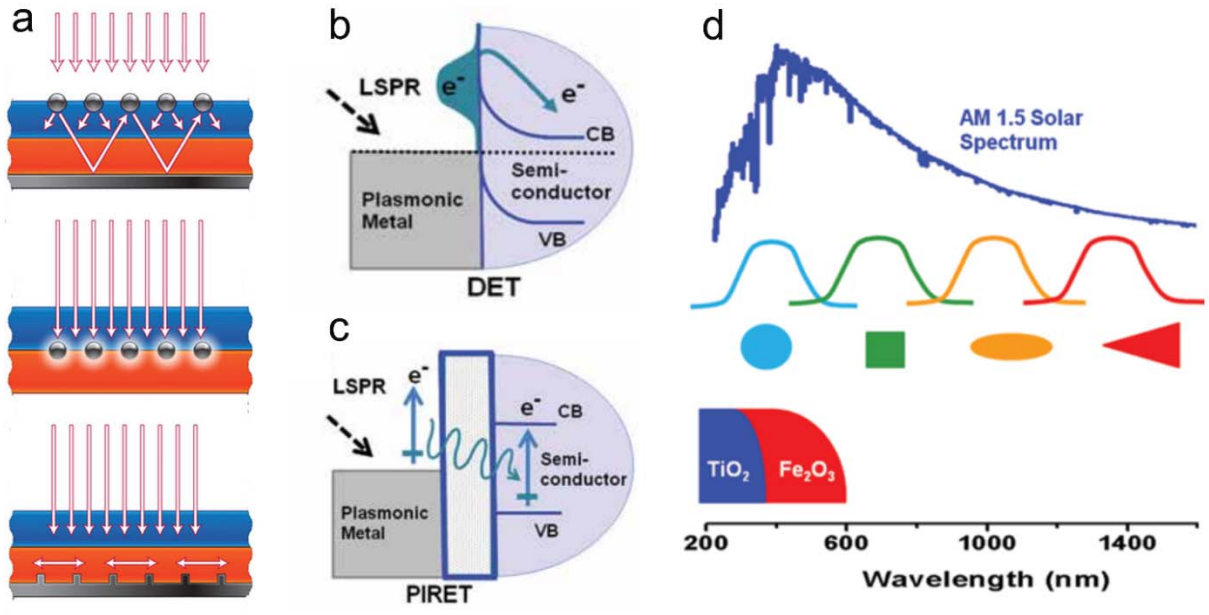

Figure 8. Photocatalysis enhancement mechanisms in plasmonic photocatalysts. (a) Illustration of the photonic enhancement. Reprinted from Ref. 190 with permission from Nature Publishing Group. (b) Direct electron transfer (DET) from the plasmonic metal to semiconductor; (c) Plasmon-induced resonant energy transfer (PIRET) from plasmonic metal to semiconductor with an insulating space layer. (d) Absorption of the full-spectrum solar radiation with multiple

plasmonic photosensitizers. (b-d) reprinted from Ref. 189 with permission from the Electrochemical Society.

Direct electron transfer (DET): Under light irradiation, conduction electrons in the plasmonic metal are excited to become highly energetic electrons, also known as hot electrons.[201-206] Hot electrons can overcome the Schottky barrier and transfer to the neighboring semiconductor (Figure 8b). Tian and Tatsuma first observed the hot electron injection to the conduction band of TiO_2 from plasmonic Au under excitation of monochromatic visible-light.[194,195] The DET process was confirmed in the Au-TiO_2,[35] Ag-Cu_2O[207] and Au-CdS[208] heterojunction systems by transient absorption spectroscopy. DET can occur with the LSPR energies below or above the band gap of the semiconductor; and its energy transfer efficiency is determined by the relative energy of hot electrons in the metal to the height of the Schottky barrier at the interface.[35,189,193,207] This differs from the electron transfer from a dye to a semiconductor, where an energetically electronic alignment is necessary for efficient downward electron transfer. In addition, the energies of hot electrons depend on the carrier concentrations and geometry (shape and size) of the plasmonic structures, which offers flexibility in controlling the DET enhancement by varying the geometry of plasmonic metals.[189,209,210]

However, it must be pointed out that the quantum efficiency in the LSPR spectrum region is two orders lower than that in the UV light region in a IPCE spectrum of metal-semiconductor composite.[211,212] One of the possible reason is that hot electron injection efficiency is only around 40% in the Au-TiO_2 composite under 550 nm excitation while the electron injection efficiency is almost 100% for ruthenium N3 dye to TiO_2.[213,214] This means some unknown pathways consume the plasmonic energy and retard its transfer to the semiconductor. More efforts are required to understand this fundamental issue in order to design efficient plasmonic photocatalysts by fully utilizing the plasmonic hot electrons.

Plasmon-induced resonance energy transfer (PIRET): When an insulating SiO_2 layer exists between the plasmonic metal and the semiconductor, the plasmon-enhanced photocatalytic activities are still observed.[196,215-220] The DET mechanism cannot occur in the presence of such an insulating layer. Recently Nick Wu's group made unprecedented discovery of the PIRET process, which has unraveled the underlying mechanism of such kind of plasmonic photocatalysis enhancement (Figure 8c).[196] PIRET proceeds via coupling between the LSPR

dipole of the plasmonic metal and the transition dipole of the semiconductor, which nonradiatively transfers the plasmonic energy from the metal to the semiconductor, leading to charge separation in the semiconductor. In contrast to DET, the dipole-dipole interaction thus does not require intimate contact between the plasmonic metal and the semiconductor. The efficiency of PIRET depends on both the distance and the spectral overlap between the semiconductor's absorption band and the SPR band of the plasmonic metal.[196] In contrast to the DET, the PIRET process is much more efficient in enhancing the photocatalytic activity. PIRET enables the charge separation in the semiconductor at the energies even below the band gap. This indicates that incorporation of multiple plasmonic photosensitizers into a wide band gap semiconductor could result in the absorption of full-spectrum solar radiation that is able to generate electron-hole pairs in the wide band gap semiconductor (Figure 8d).

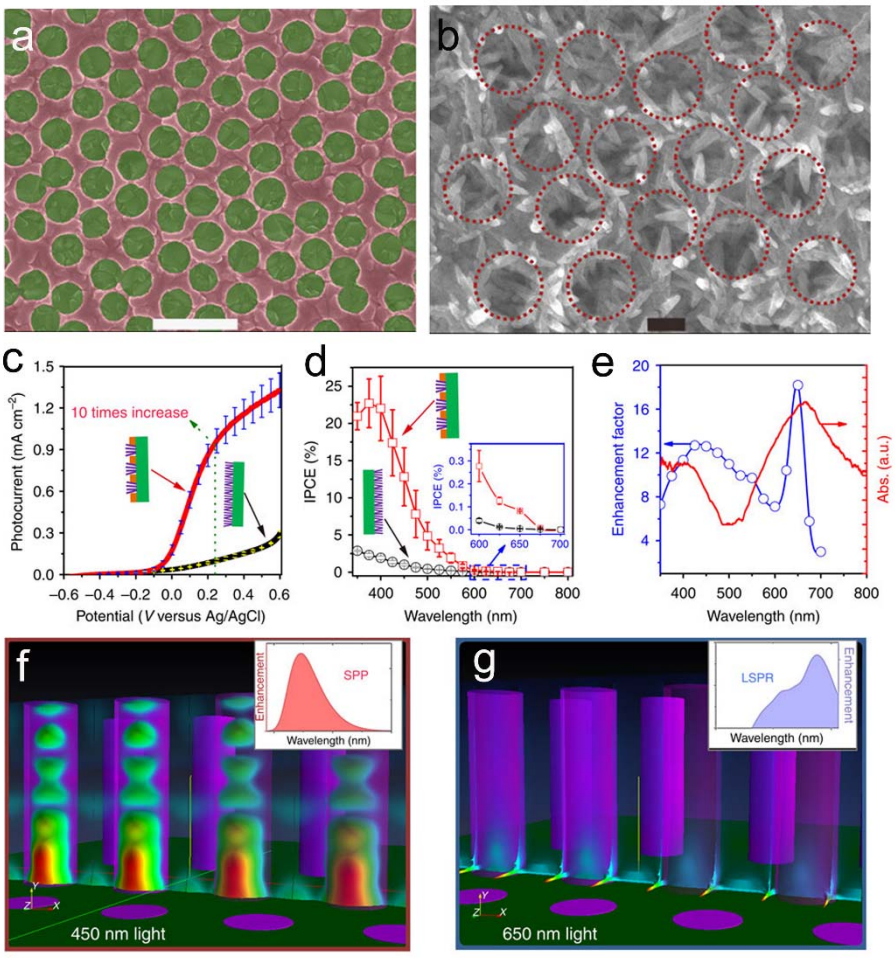

Figure. 9 Enhancement of solar water splitting by hematite nanorod array with a plasmonic Au nanohole array pattern. (a&b) SEM images of the Au nanohole array pattern before and after

growth of the hematite nanorod array, (c-e) the photoelectrochemical performances including J-V curve, IPCE spectra and IPCE enhancement spectrum, (f) The SPP-associated light trapping in the hematite nanorod, (g) The LSPR on the edge of the nanoholes. Reprinted from Ref. 193 with permission from Nature publishing Group.

Although plasmonic nanostructures have a large extinction cross-section, which can effectively absorb the sunlight,[189,221] most of the plasmonic metal-semiconductor heterojunction photocatalysts reported previously have exhibited a low efficiency in the spectral range of SPR because the large amount of plasmonic energy in the metal is not able to efficiently transfer to the semiconductor. Nick Wu's group recently designed a plasmonic metal-semiconductor heterojunction photoelectrode to address this challenge, as shown in Figure 9.[193] A long-range ordered gold nanohole array was fabricated on a FTO substrate, which enabled both SPP and LSPR modes simultaneously under the solar radiation (Fig. 9a). A hematite nanorod array was grown onto the plasmonic gold nanohole array pattern (Fig. 9b). The photoelectrochemical water splitting performance of the hematite nanorod was significantly improved by the plasmonic nanostructure, leading to a ten-fold increase in the photocurrent at 1.23 V (*vs.* RHE) (Fig. 9c). The IPCE enhancement spectrum (Fig. 9d&e) has revealed two enhancement wavelength ranges, which corresponded to the SPP and LSPR enhancements, respectively. The SPP launched a guided mode inside the hematite nanorods to increase the light absorption in hematite above the band gap (Fig. 9f). Also, the Au nanohole initiated a LSPR mode, which enhanced the charge separation in hematite below the band gap via the PIRET process (Fig. 9g). Moreover, the charge carrier lifetime in hematite was prolonged by the intense local plasmonic field at the metal/hematite interface, which reduced the charge recombination rate in hematite. In addition, Wang and his coworkers have assembled Au nanocrystals on the TiO_2-based photonic crystal substrate.[124] A high IPCE efficiency of nearly 8% in SPR spectral range was achieved. It is worth noting that the maximum values of both IPCE and photocurrent occurred when the photonic crystal band gap matched the LSPR band of Au.

4.2 Dye-Sensitized Semiconductors

Wide band gap semiconductors have the limited light absorption spectral range despite a lot of other advantages. Hence they are photosensitized with organic dyes to harvest the visible-light.

Similar to the dye-sensitized solar cells, the dyes are excited to the excitation status (S^*) after harvesting the visible-light that cannot be absorbed by the wide band gap semiconductor. The photo-generated electrons are then injected to the conduction band of the semiconductor.[36,37] To make the charge transfer energetically favorable, the lowest unoccupied molecular orbital (LUMO) of the dye must be higher than the conduction band of the semiconductor, while the highest occupied molecular orbital (HOMO) lies between the valence band of semiconductor and the oxidation reaction potential. After donating electrons, the dyes become unstable and must be regenerated quickly with an electron donor. The choice of the electron donor is important because it not only prevents the dyes from being etched during the photoelectrochemical reaction but also determines the open voltage for the whole system. One of challenges is that the charge recombination competes with the electron injection process to consume the charge carriers.[36] Another concerns is the instability of dyes under long-term irradiation of the sunlight, especially the UV photons.

4.3 Semiconductor-Semiconductor Heterojunctions

Two different inorganic semiconductors are joined together to form a heterojunction, which has been demonstrated to bring great benefit to photocatalysis in four ways: (i) broadening the light absorption spectral range, (ii) enhancing the charge separation, (iii) suppressing the charge recombination, (iv) preventing the narrow band gap semiconductor from photo-corrosion.

When two materials that have the band gap close to each other, such as n-type $SrTiO_3$ (E_g=3.3 eV) and n-type TiO_2 (E_g=3.2 eV), form a heterojunction, the light absorption spectral range of materials is not affected. But the band offset can improve the charge separation and inhibit the charge recombination.[222-224] This has been confirmed by a shift in the Fermi level to the negative potential direction, implying more accumulation of electrons in the coupled heterostructure. [223]

When two semiconductors form a *p*-*n* junction, a stronger electric field is generated at the interface, which results in more significant improvement in the charge separation and the reduction of the charge recombination rate.[49,225-228] For example, the *p*-type NiO nanoparticles[49] and the *p*-type Mg-doped hematite[226] have been grown on a *n*-type hematite thin film to form *p*-*n* junction photoanodes for solar water splitting, respectively. The p-type outer layer not only facilitates the extraction of accumulated holes from hematite, but also lowers the barrier for

oxygen evolution reaction with negative shift of the onset potential.[49,226,227]

Another type of popular heterojunction is formed by a wide band gap semiconductor (such as TiO_2, $K_4Nb_6O_{17}$ and $SrTiO_3$) with a narrow band gap semiconductor (such as CdS, CdSe and PbS quantum dots), in which the quantum dots with high absorption coefficient function as a photosensitizer.[89,90,100,106,233-237]. Other examples include *p*-type Cu_2O (E_g=2.2eV)/*n*-TiO_2 (E_g =3.2eV)[229,230], *p*-type $CaFe_2O_4$ (E_g =1.9eV)/*n*-type $ZnFe_2O_4$ (E_g =2.0eV) and $MgFe_2O_4$ (E_g =2.0eV) /$PbBi_2Nb_{1.9}W_{0.1}O_9$ (E_g =2.75eV).[225,231,232] In the QD/semiconductor systems, the light absorption spectral range of QDs, which is dependent on the band gap, can be easily tuned to the infrared range by reducing the QD size. A favorable band gap alignment is required to be Type-II band offset in order to enable the efficient charge transfer, as shown in Figure 10a. The conduction band and the valance band of the narrow band gap semiconductor should have higher energy level than those of the wide band gap semiconductor. The drive force of interfacial charge transfer depends on the band offset.[237] Figure 10b shows the tuning of band alignment and the interfacial charge transfer between TiO_2 and PbS QDs by tailoring the QD size. Smaller QDs have a larger band-gap and a higher conduction band level, leading to faster electron transfer to TiO_2. The electron transfer is disabled from the QDs to TiO_2 when the conduction band of QDs is lower than that of TiO_2, as shown in Figure 10b.[237] This experiment clearly demonstrated the importance of proper band alignment to the interfacial charge transfer in the composite. Li and his co-workers have created a multi-junctioned CdS@anatase TiO_2@Rutile TiO_2 structure as the photoelectrode.[106] Inserting anatase TiO_2 layer as the mediator, which has a conduction band level lower than that of CdS, but slightly higher than that of rutile TiO_2, results in an excitation staircase alignment. This band alignment directs a gradual staircase electron transfer from CdS through anatase TiO_2 to the rutile TiO_2 nanorod with a interfacial potential gradient, while blocks their backward transfer to CdS. This ternary system exhibited the photocurrent twice than the binary CdS@rutile TiO_2 system. A similar structure has also been successfully used in the ternary CdS/TiO_2/WO_3 system with a photocurrent about 5 times larger than that of sole CdS and about 2-3 times larger than that of the binary composite.[238] The staircase structure in a multi-junction guides the charge carriers to move in the desired direction, which is an effective strategy to improve the photocatalysis efficiency.[106,238-240]

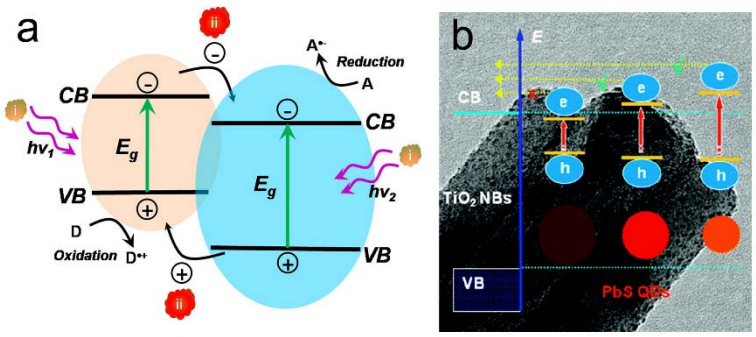

Figure 10. (a) Desirable Type-II band alignment and the charge separation and transfer processes in the composite photocatalyst; (b) Size-dependent band alignment and the charge transfer in PbS/TiO_2. Reprinted from Ref. 237 with permission from American Chemical Society.

In organic dye-sensitized metal oxide composites, the photo-generated electrons in the dye can be quickly injected into the conduction band of metal oxide. However, slow electron injection and high charge recombination rate at the interface is of major concern regarding the QD-metal oxide composites.[241-243] The previous studies show that the interfacial trap states and the back transfer in the heterojunction are responsible for the loss of charge transfer efficiency.[35] In particular, the trap states lead to a high Auger scattering rate at the interface, consuming the photo-generated charge carriers.[35,244-246] It has been reported that the Au nanoparticles sandwiched between the TiO_2 nanorod core and the CdS shell can reduce the trap-state Auger scattering rate, suppress the back transfer of photo-generated electrons, and expedite the interfacial charge carrier transfer from CdS to TiO_2.[35] Another concern regarding the metal chalcogenide QD-sensitized metal oxide is the photocorrosion of metal chalcogenide because of the photo-oxidation in water under sunlight. High concentration of polysulfide aqueous electrolyte (0.25 M Na_2S and 0.35 M Na_2SO_3, *pH* 12) is typically employed to consume the photo-generated holes to protect the sulfide semiconductors.

Generally wide band gap semiconductors are photoelectrochemically stable but can only absorb the UV light of solar radiation while narrow band gap conductors have a wide spectral range of light absorption but many of them suffer from photo-corrosion. Hence a narrow band gap semiconductor is coated with an outer layer of wide band gap semiconductor to isolate the narrow band gap semiconductor from the liquid electrolyte. Such a composite can achieve a wide spectral range of light absorption and long-term photo-stability. For instance, Cu_2O is a *p*-type

semiconductor with a direct band gap of 2 eV; and it has a minority carrier diffusion length of 20-100 nm and an optical absorption depth of 10 μm.[247] To solve its instability problem, a multi-layered FTO/Au/Cu_2O/Al-doped ZnO/TiO_2 photocathode was created, in which TiO_2 was the outmost layer.[247] This multi-layered photocathode has achieved a photocurrent density of 7.6 mA/cm^2 at 1.23 V (vs. RHE). Two other examples are the *p*-type Si/*n*-type Fe_2O_3 core-shell nanowire photoanode [248] and the *n*-type Si/*n*-type TiO_2 core-shell nanowire photoanode [249]. In the latter case, the TiO_2 shell prevents the Si nanowire from photo-corrosion and absorbs the UV-light in the solar radiation, and allows the visible-light pass while the Si nanowire absorbs the visible-light.

4.4 Semiconductor-Carbon Composites

Various forms of carbon materials including amorphous carbon, graphite-like carbon, fullerene, carbon nanotubes, graphene and graphene oxide have been coupled with semiconductors to form composites in order to improve the photocatalytic activity. 1D carbon nanotubes have been used as the scaffold for supporting TiO_2 [250-252] and other semiconductors, which can increase the specific surface area of semiconductor photocatalysts. In addition, the carbon nanotubes provide the charge transport channels, which can reduce the charge recombination rate.

Recently many attempts have been made to couple semiconductors to 2D graphene or graphene oxide to form heterogeneous photocatalysts.[253-257] Graphene sheets have very high specific surface area (~2,600 m^2/g) [258] and act as excellent physical supports for semiconductor photocatalysts. The graphene/semiconductor photocatalysts exhibit better photocatalytic activity compared to the semiconductor alone. Transient absorption spectroscopy and time-domain terahertz spectroscopy were recently obtained from the reduced graphene oxide (rGO)-Fe_2O_3 composite.[259] The spectroscopic results have provided the direct evidence that the photo-generated electrons transfer as the mobile carriers into the rGO sheets from α-Fe_2O_3, which can migrate and are trapped, reducing the charge recombination rate. It is worth noting that the interfacial electron transfer rate between TiO_2 and the graphene sheet is dependent on dimensionality of semiconductor.[260] 0D nanoparticles, 1D nanotubes and 2D nanosheets of TiO_2 were supported on the 2D graphene sheet, respectively. The interfacial electron transfer rate was ranked as 0D-2D<1D-2D<2D-2D.

It is interesting that graphene oxide or rGO can be tuned to either *p*-type or *n*-type semiconductor by doping different elements. Nick Wu's group took this advantage to prepare the *p*-MoS_2/*n*-rGO composite, in which multiple nanoscale *p*-*n* junctions were formed in a single nitrogen-doped rGO sheet (Figure 11a). [228] The free-standing solitary MoS_2 nanoparticles showed negligible photocatalytic activity toward hydrogen evolution (Figure 11b). In contrast, the MoS_2/rGO composite where the MoS_2 nanoplatelets were supported on the undoped rGO sheets showed evident photocatalytic activity. The *p*-MoS_2/*n*-rGO composite exhibited much higher photocatalytic activity. Photocurrent transient study shows that the layer-structured *p*-*n* junction greatly enhances the charge separation and suppresses the charge recombination. Besides graphene as the physical support for semiconductor, it can bridge two semiconductors. Feng and her co-workers have employed graphene as the interlayer between the α-Fe_2O_3 nanorod and the $BiV_{1-x}Mo_xO_4$ shell.[261] The graphene "bridge" has promoted the interfacial charge transfer between two semiconductors.

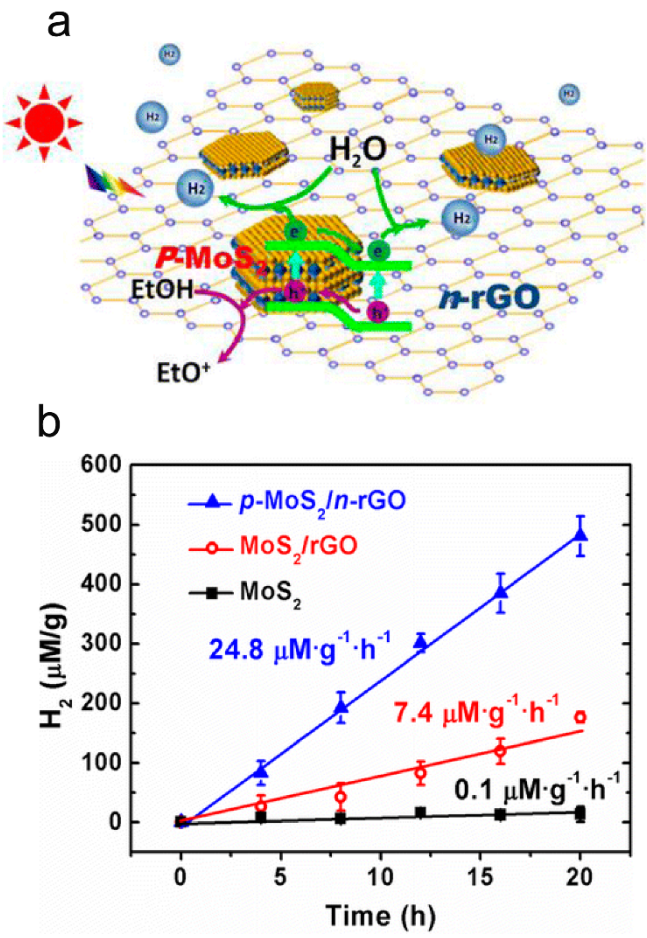

Figure 11. (a) Schematic illustration of the *p*-MoS_2/*n*-rGO composite photocatalysts; (b)

Hydrogen evolution by the MoS_2, the MoS_2/rGO and the *p*-MoS_2/*n*-rGO photocatalysts. Reprinted from Ref. 228 with permission from American Chemical Society.

4.5 Multijunctions, Tandem Cells and Z-Schemes

Multijunctions and tandem cells for solar fuel generation are similar to those used in photovoltaic devices. In a multijunction with a series connection, the overall photovoltage is the sum of individual junctions but the overall photocurrent is determined by the minimum among all the individual junctions.[147] The individual junctions absorb the sunlight in different spectral ranges that are complementary to each other. Hence the overall light absorption spectral range of a multijunction-based PEC is greatly extended. In short, a multijunction-based PEC can achieve much higher solar energy conversion efficiency than a single-junction-based PEC because of its higher photovoltage and larger light absorption spectral range.[21-23,262,263] Tandem PEC cells has a multijunction design that consists of a photoanode|photocathode or a photoelectrode|photovoltaic configuration with a tunnel junction. Multijunction PEC cells based on III-V or Si hold the world record of STH efficiency up to 18%.[22] As mentioned above, high cost and instability are two main issues to restrict its practical application. Effort is being made to replace the expensive materials in tandem cells with inexpensive earth-abundant elements. Nocera et al. have developed an amorphous silicon based triple junction PEC with earth-abundant metals and Co-Pi as the catalyst. The cell has achieved an efficiency of 4.7% for solar water splitting.[263] Recently Sivula and his coworkers have successfully constructed a tandem cell with hematite or WO_3 as the photoanode, as shown in Fig. 12a. The cell reached a STH efficiency of 3.1%.[262] All the semiconductors used were earth-abundant.

The concept of "Z-scheme" photocatalyst comes from the natural photosynthesis system in green plants.[264] A "Z-scheme" can be considered as a special type of PEC-PEC tandem cell, in which two semiconductors are bridged with a redox mediator (Fig. 12b). Two photocatalysts are excited simultaneously to generate electron-hole pairs. The electrons from the conduction band of one photocatalyst and the holes from valance band of another photocatalyst will be consumed with the redox mediator. Hence the water reduction reaction and the water oxidation reaction occur separately on each photocatalyst.[13,265-267] The Z-scheme design has some characteristics as follows:[13,265-267]

(i) Combination of two different semiconductor photocatalysts allows the broad light absorption.

Furthermore, light is utilized more efficiently compared to single semiconductor because the energy required to drive each photocatalyst is reduced.[266]

(ii) Consumption of photo-generated electrons and holes with the redox mediator significantly reduces the charge recombination in the semiconductors, which improves the photocatalytic efficiency.

(iii) Each photocatalyst in a Z-scheme is responsible only for half reaction of the water splitting but larger driven force is available for the reduction and oxidation reactions.

(iv) The semiconductors with the band edge energetics only for either H_2 or O_2 evolution can be involved as the counter partner for overall water splitting in this system. For example, WO_3 with a conduction band level lower than the H_2O/H_2 potential has proven being effective when coupled with $SrTiO_3$:Rh in a Z-scheme for overall water splitting.[268]

However, some issues still need to be addressed for the Z-scheme photocatalysts. Only limited semiconductor photocatalysts are available for construction of a Z-scheme. These include $SrTiO_3$, TaON, and $BaTaO_2N$ for the water reduction reaction; WO_3 and $BiVO_4$ for the water oxidation reaction.[268-276] Few studies have reported the possibility of TiO_2 as H_2 or O_2 photocatalyst in the Z-scheme system.[277,278] Further work needs to be performed to explore more semiconductors to construct the Z-scheme. In addition, the most commonly used redox couples in Z-scheme systems such as IO^{3-}/I^- and Fe^{3+}/Fe^{2+} are liquid and have shown the negative effects (back reactions and strong visible light absorption).[240,266]

To solve these problems, Kudo *et al.* have reported a Z-scheme system Ru-$SrTiO_3$:Rh||$BiVO_4$ for overall water splitting but without employment of additional redox couples.[275] It is believed that the impurity level (Rh^{3+}/Rh^{4+}) formed by Rh doping in the forbidden gap functions as a mediator to assist the electron transfer in this system. Another approach is to employ a solid-state electron mediator for replacing the liquid redox couples. Graphene oxide and Au nanoparticles have been claimed being effective to shuttle the electrons between two semiconductors for the improved photocatalytic activity due to their high electron conductivity. [279-281]

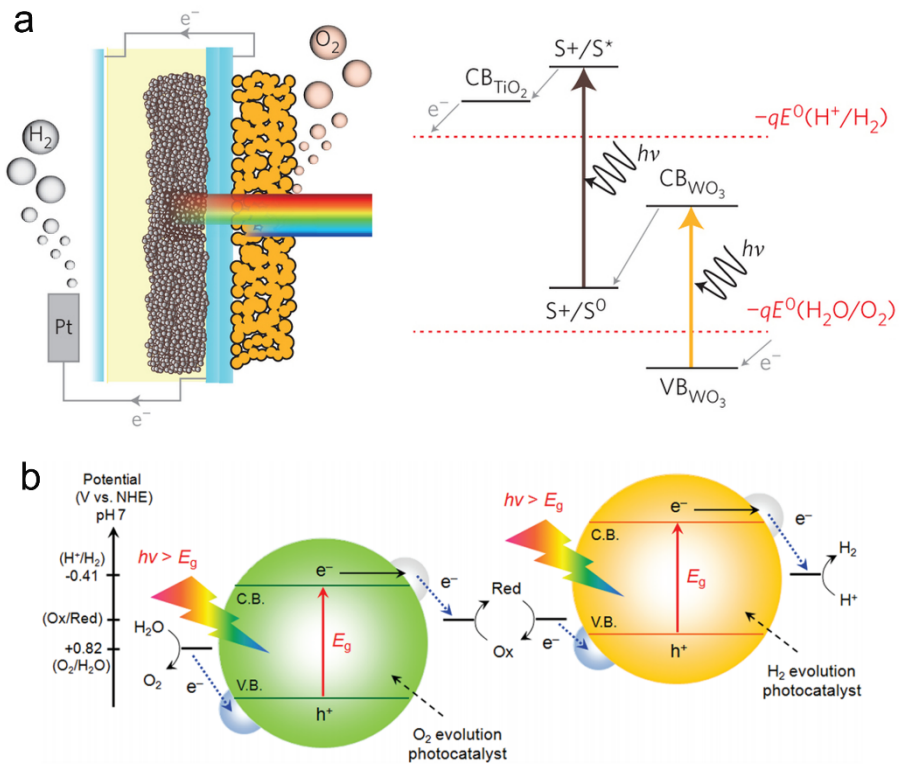

Figure 12. Charge transfer in (a) tandem cell and (b) Z-scheme photocatalysis systems. Reprinted from Ref. 262 with permission from Nature publishing group and Ref. 265 with permission from American Chemical Society.

4.6 Co-catalysts

Although a lot of semiconductors have been explored for photocatalysts/photoelectrodes for water splitting, most of them show insufficient catalytic or electrocatalytic activity toward redox reactions.[10-13,180,225,240,282] It is therefore essential to deposit co-catalysts on the surface of photocatalysts/photoelectrodes in order to lower the overpotential/activation energy of the redox reaction and to avoid the back reactions. In many cases, co-catalysts help extract the photo-generated minority charge carriers inside the semiconductor to the surface, and provide the active sites for surface redox reactions. For water splitting, the co-catalysts for the hydrogen evolution reaction (HER) are different from those for the oxygen evolution reaction (OER). The electrocatalytic activity of co-catalysts can be initially screened with the assistance of a volcano plot for either HER or OER, as shown in Figure 13. [283,284]. The co-catalysts that are close to the apex of the volcano curve generally possess relatively high activity toward a specific reaction. Good co-catalyst can effectively shift the photocurrent onset potential in the *J-V* curve as shown

in Figure 1c. In addition, the stability of co-catalysts needs to be evaluated. Co-catalyst may change under a large applied potential. The impurity in the electrolyte may poison the co-catalysts. In addition, the chemical diffusion at the semiconductor/co-catalyst interface may occur under the long-term operation. One also needs to pay attention to the mass loading and thickness of the deposited co-catalyst on the semiconductor surface. Too high mass loading or too thick film of co-catalyst could block the light incident to the semiconductor because co-catalysts are typically opaque. Transparent co-catalysts are rare although we wish to have. However, a photoactive co-catalyst that has a light absorption spectral range complementary to that of the underneath semiconductor could be an alternative solution. For example, MoS_2 not only catalyzes the HER but also is photoactive if coupled to a good charge carrier shuttle. [228]

Oxygen Evolution Reaction (OER) Co-catalyst: The water oxidation half reaction is a four-electron transfer process. The slow kinetics of OER limits the efficiency of both photon-driven and electricity-driven water splitting. Trasatti has obtained a volcano plot of electrocatalytic OER on the selected metal oxides. [285] Rossmeisl and his co-workers have used the computation method to obtain a volcano plot for an expanded list of metal oxides (Figure 13 a). [283] It can be seen from the volcano plot that the representative OER catalysts are IrO_2, RhO_2, NiO, CoO_x and MnO_x.[225,286] IrO_2 is considered as the best OER co-catalyst because of its strong activity and the lowest overpotential for electrocatalytic water oxidation.[86] A shift of 200 mV in the photocurrent-onset potential was observed when it was deposited on the hematite photoanode for water oxidation.[48] However, its high cost is of major concern. As a result, some low-cost, earth-abundant materials, such as nickel oxides and cobalt oxides have been investigated as the OER catalyst. But they show relatively low cathodic shift in the photocurrent-onset potential.[49,287,288] Fortunately, cobalt phosphate (Co-Pi) has demonstrated negative shift at a neutral pH, which is comparable to IrO_2.[289] The largest cathodic shift in the onset potential up to 440 mV was obtained by incorporating Co-Pi with the W-doped $BiVO_4$ photoanode.[290] After its emergence, Co-Pi has been intensively coupled with many photoanode materials such as hematite, ZnO, $BiVO_4$, TiO_2, WO_3 and other semiconductors for water oxidation.[290-294] Co-Pi catalyst can efficiently collect and store photo-generated holes from the photoanode semiconductor, reducing the surface charge recombination rate. [290] In addition, an α-FeOOH thin film has been demonstrated as the OER catalyst. Its activity could be comparable to that of other OER co-catalyst such as Co-borate on the amorphous Si electrode.[295,296] When FeOOH was coupled

with NiOOH to form a dual layer on the porous $BiVO_4$ electrode, the OER catalyst layer not only greatly reduced the interfacial charge recombination at the electrode/OER catalyst junction, but also created a Helmholtz layer potential drop at the OER catalyst/electrolyte junction, which resulted in 2.73 mA/cm^2 at 0.6 V (*vs*. RHE), the highest photocurrent density for the $BiVO_4$ photoanode so far.[61]

Hydrogen Evolution Reaction (HER) Co-catalysts: Trasatti has experimentally measured the volcano plot of electrocatalytic HER on the selected metals.[297] Recently, MoS_2 and Ni_2P were added into this volcano plot as shown in Figure 13b. [284] Representative HER catalysts are noble metals such as Pt, Rh, Ru and Pd. The intimate contact between the semiconductor and the noble metal leads to the formation of a Schottky junction.[225] The electric field formed in the Schottky junction acts as the electron sink to trap the photo-generated electrons transferred from the semiconductor. The trapping ability is largely dependent on the work functions of the noble metals.[286] Platinum has the largest work function (6.35 eV), and rendered it the best choice as the co-catalyst. The trapped electrons are quickly discharged across the interface for the catalytic proton reduction.[298] It is worth noting that noble metals such as Pt and Rh, which catalyze the HER, may also catalyze the back reaction, leading to the formation of H_2O. To address this issue, Domen's group has developed a Ph@Cr_2O_3 core-shell nanoparticle as the HER co-catalyst on the GaN:ZnO photocatalyst, in which the Cr_2O_3 shell allows the proton and H_2 molecule to pass through, but blocks the oxygen species. [299]

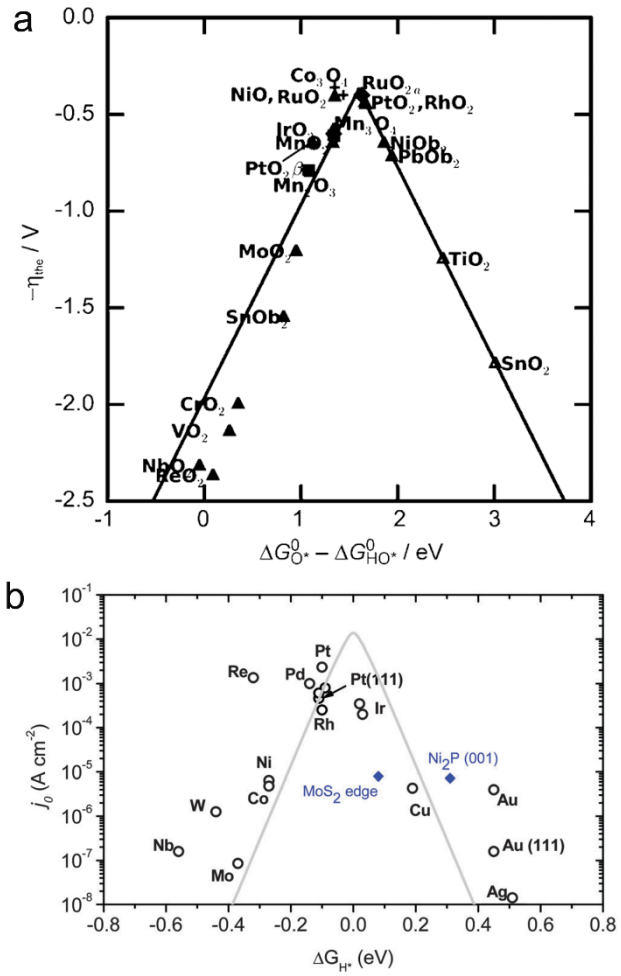

Figure 13. (a) Volcano plot of oxygen evolution reaction on metal oxides, Reprinted from Ref. 283 with permission from John Wiley; (b) Volcano plot of hydrogen evolution reaction, Reprinted from Ref. 284 with permission from Royal Society of Chemistry.

Unfortunately, the scarcity and high cost of the noble metals limit their commercial application. It is crucial to search for inexpensive, earth-abundant co-catalysts for HER. Recently, MoS_2, which is an earth-abundant semiconductor, has arisen as an active HER catalyst with a potential to fill this void.[228,300-309] MoS_2 has an intrinsic layered structure stacked by S-Mo-S sheets with Van der Waals MoS_2 into nanostructures with more exposed active edges can improve its catalytic activity. As described above, MoS_2 is also a photoactive material. Although it alone has no photocatalytic activity, the *p*-MoS_2/*n*-rGO composite exhibits strong visible-light photocatalytic activity toward water reduction to hydrogen. [228] WS_2 and NiS have also attracted attention because of their similar structure to MoS_2.[310,311] A different molybdenum sulfide,

Mo_3S_4, is also an effect HER catalyst. A negative shift of the proton reduction overpotential up to 0.7 V was observed when Mo_3S_4 was deposited on the *p*-Si photoanode in a PEC cell.[304]

5. Conclusions and Perspective

As described above, wide band gap semiconductors such as TiO_2 are inexpensive and stable but not effective in absorption of visible-light. Narrow band gap semiconductors such as CdS and III-IV compounds have a potential to achieve high efficiency but suffer from instability and high cost. In addition, charge recombination is one of critical factor that limits the solar energy conversion efficiency of photocatalysts and PECs.

Development of inexpensive, stable and highly efficient photocatalyst/photoelectrode materials is the key to the commercialization of photocatalysts and PECs for solar fuel production. In the last decade, we have witnessed lots of innovations in the structure design and the material combination, which is built on the significant progress in understanding of the correlation of the photocatalytic/photoelectrochemical performance of semiconductors with the material feature and five vital processes including light absorption, charge separation, migration and recombination as well as (electro)catalytic activity. Such fundamental research still needs to move forward before one can develop photocatalysts/photoelectrodes in a fashion of "material-by-design". Combination of computation, ultrafast optical spectroscopy, microscopic characterization and electrochemical technique will expedite the mechanistic studies on the nanometer, atomic and electronic levels. In authors' personal opinion, new development on single materials in the near future should be put more emphasis on the intrinsic "narrow-band-gap" semiconductors or those with tunable band gap via alloying or forming a solid solution. For composite materials, "wide-band-gap" semiconductors could still play significant role as one of components in the whole system. It is of particular interest that plasmonic nanostructures can overcome the band edge energetics constraint of single semiconductors, and harness the sunlight below the band gap of semiconductor to induce the charge separation. Hence plasmonic metal-semiconductor composites hold great promise in photocatalysts/photoelectrodes. In addition, multi-junctions and tandem cells are promising but a spot light will be put on lowering their costs.

Last but not least, one can envision further exploration of green synthesis and earth-abundant materials for photocatalysts and PECs in order to address the challenges in the cost and sustainability.

Acknowledgments

This work was supported by the National Science Foundation (CBET-1233795). Acknowledgment is also made to the Donors of the American Chemical Society Petroleum Research Fund (PRF# 53490-ND10) for partial support of this research. J. Li thanks Mr. Scott Cushing for running the simulation of theoretical STH efficiency in Figure 2.

References

[1] International Energy Agency in World Energy Outlook 2011, http://www.worldenergyoutlook.org, 2011.

[2] *Key World Energy Statistics*. http://www.iea.org/publications/freepublications/publication/KeyWorld2013.pdf, 2013.

[3] F. E. Osterloh and B. A. Parkinson, *MRS Bulletin*, 2011, **36**, 17-22.

[4] S. H. Habisreutinger, L. Schmidt-Mende and J. K. Stolarczyk, *Angew. Chem. Int. Ed.*, 2013, **52**, 7372-7408.

[5] N. S. Lewis, and D. G. Nocera, *Proc. Natl. Acad. Sci. USA,* 2006, **103**, 15729-15735.

[6] N. S. Lewis, *Science*, 2007, **315**, 798-801.

[7] B. Norton. *Harnessing Solar Heat*. Springer, **2013**.

[8] M. Grätzel, *Nature*, 2001, **414**, 338-344.

[9] M. Grätzel, *J. Photochem. Photobiol. C: Photochem. Rev.*, 2003, **4**, 145-153.

[10] (*a*) X. Chen, C. Li, M. Grätzel, R. Kostechi, and S. S. Mao, *Chem. Soc. Rev.*, 2012, **41**, 7909-7937. (*b*) S. Chen and L. Wang, *Chem. Mater.*, 2012, **24**, 3659-3666.

[11] M. G. Walter, E. L. Warren, J. R. Mckone, S. W. Boettcher, Q. Mi, E. A. Santori and N. S. Lewis, *Chem. Rev.,* 2010, **110**, 6446-6473.

[12] T. Hisatomi, J. Kubota and K. Domen, *Chem. Soc. Rev.*, 2014, DOI:10.1039/C3CS60378D.

[13] A. Kudo and Y. Miseki*, Chem. Soc. Rev.*, 2009, **38**, 253-278.

[14] E. F. Benson, C. P. Kubiak, A. J. Sathrum and J. M. Smieja, *Chem. Soc. Rev.*, 2009, **38**, 89-99.

[15] J. Scheneider, H. Jia, J. T. Muckerman and E. Fujita, *Chem. Soc. Rev.*, 2012, **41**, 2036-2051.

[16] X. Huang, S. Han, W. Huang and X. Liu, *Chem. Soc. Rev.*, 2013, **42**, 173-201.

[17] A. Fujishima and K. Honda, *Nature*, 1972, **238**, 37-38.

[18] T. Inoue, A. Fujishima, S. Konishi and K. Honda, *Nature*, 1979, **277**, 637-638.

[19] DOE, *Hydrogen Production Technical Team Roadmap*, **2013**.
http://www1.eere.energy.gov/vehiclesandfuels/pdfs/program/hptt_roadmap_june2013.pdf.

[20] DOE, Photoelectrochemical Hydrogen Production: DOE PEC Working Group Overview, **2011**. http://www.hydrogen.energy.gov/pdfs/progress10/ii_g_1_miller.pdf.

[21] O. Khaselev and J. A. Turner, *Science*, 1998, **280**, 425-427.

[22] S. Licht, B. Wang, S. Mukerji, T. Soga, M. Umeno and H. Tributsch, *Int. J. Hydrogen Energy* 2001, **26**, 653-659.

[23] J. R. Bolton, S. J. Strickler and J. S. Connolly, *Nature*, 1985, **316**, 495-500.

[24] M. R. Hoffman, S. T. Martin and W. Choi, *Chem. Rev.*, 1995, **95**, 69-96.

[25] A. L. Linsebigler, G. Q. Lu and J. T. Yates, *Chem. Rev.*, 1995, **95**, 735-758.

[26] A. Mills and S. J. Hunte, *J. Photochem. Photobiol. A*, 1997, **108**, 1-35.

[27] A. Fujishima, X. T. Zhang and D. A. Tryk, *Surf. Sci. Rep.*, 2008, **63**, 515-582.

[28] R. Leary and A. Westwood, *Carbon*, 2011, **49**, 741-772.

[29] *Impedance spectroscopy Theory, experimental, and Applications,* ed. E. Barsoukov, J. R. Macdonald, 2nd Ed. John Wiley, New Jersey, 2005.

[30] W. Fan, Q. Zhang and Y. Wang, *Phys. Chem. Chem. Phys.*, 2013, **15**, 2632-2649.

[31] N. Serpone, D. Lawless and R. Khairutdinov, *J. Phys.Chem.*, 1995, **99**, 16646-16654.

[32] N. Serpone, G. Sauve, R. Koch, H. Tahiri, P. Pichat, P. Piccinini, E. Pelizzetti and H. Hidaka, *J. Photochem. Photobiol. A*, 1996, **94**, 191-203.

[33] *Photoelectrochemical Water Splitting: Standards, Experimental Methods, and Protocols*, ed. Z. Chen, H. Dinh and E. Miller, Springer, New York, 2013.

[34] D. Tafalla, P. Salvador and R. M. Benito, *J. Electrochern. Soc.*, 1990, **137**, 1810-1815.

[35] J. Li, S. K. Cushing, P. Zheng, T. Senty, F. Meng, A. D. Bristow, A. Manivannan and N. Q. Wu, *J. Am. Chem. Soc.,* 2014, **136**, 8438-8449.

[36] W. J. Youngblood, S. A. Lee, K. Maeda and T. E. Mallouk, *Acc. Chem. Res.*, 2009, **42**, 1966-1973.

[37] J. R. Swierk and T. E. Mallouk, *Chem. Soc. Rev.*, 2013, **42**, 2357-2387.

[38] Y. Xu, and M. A. A. Schoonen, *Am. Mineral.*, 2000, **85**, 543-556.

[39] E. Halary-Wagner, F. Wagner and P. Hoffmann, *J. Electrochem. Soc.*, 2004, **151**, C571-C576.

[40] M. Takahashi, K. Tsukigi, T. Uchino and T. Yoko, *Thin Solid Film.,* 2001, **388**, 231-236.

[41] P. J. Salvador, *Appl. Phys.*, 1984, **55**, 2977-2985.

[42] I. Balberg and H. Pinch, *J. Magn. Magn. Mater.*, 1978, **7**, 12-15.

[43] K. M. H. Young, B. M. Klahr, O. Zandi and T. W. Hamann, *Catal. Sci. Technol.*, 2013, **3**, 1660-1671.

[44] A. B. Murphy, P. R. F. Barnes, L. K. Randeniya, I. C. Plumb, I. E. Grey, M. D. Horne and J. A. Glasscock. *Int. J. Hydrogen Energy*, 2006, **31**, 1999-2017.

[45] M. J. Katz, S. C. Riha, N. C. Jeong, A. B. F. Martinson, O. K. Farha and J. T. Hupp, *Coord. Chem. Rev.*, 2012, **256**, 2521-2529.

[46] K. Sivula, F. L. Formal and M. Grätzel, *ChemSusChem,* 2011, **4**, 432-449.

[47] T. W. Hamann, *Dalton Trans.*, 2012, **41**, 7830-7834.

[48] S. D. Tilley, M. Cornuz, K. Sivula and M. Grätzel, *Angew. Chem. Int. Ed.*, 2010, **49**, 6405-6408.

[49] J. Li, F. Meng, S. Suri, W. Ding, F. Huang and N. Wu, *Chem. Comm.*, 2012, **48**, 8213-8215.

[50] J. Y. Kim, G. Magesh, D. H. Youn, J. Jang, J. Kubota, K. Domen and J. S. Lee, *Sci. Rep.*, 2013, **3**, 2681.

[51] L. Zhang, E. Reisner and J. J. Baumberg, *Energy Environ. Sci.,* 2014, **7**, 1402-1408.

[52] Y. Park, K. L. McDonald and K. Choi, *Chem. Soc. Rev.*, 2013, **42**, 2321-2337.

[53] A. Walsh, Y. Yan, M. N. Huda, M. M. Al-Jassim and S. H. Wei, *Chem. Mater.*, 2009, **21**, 547-551.

[54] S. J. Hong, S. Lee, J. S. Jang and J. S. Lee, *Energy Environ. Sci.*, 2011, **4**, 1781-1787.

[55] J. A. Seabold, K. Zhu and N. R. Neale, *Phys. Chem. Chem. Phys.*, 2014, **16**, 1121-1131.

[56] Z. Li, W. Luo, M. Zhang, J. Feng and Z. Zou, *Energy Environ. Sci.*, 2013, **6**, 347-370.

[57] D. K. Zhong, S. Choi and D. R. Gamelin, *J. Am. Chem. Soc.*, 2011, **133**, 18370-18377.

[58] F. F. Abdi and R. van de Krol, *J. Phys. Chem. C*, 2012, **116**, 9398-9404.

[59] W. Luo, Z. Yang, Z. Li, J. Zhang, J. Liu, Z. Zhao, Z. Wang, S. Yan, T. Yu and Z. Zou, *Energy Environ. Sci.*, 2011, **4**, 4046-4051.

[60] S. K. Pilli, T. E. Furtak, L. D. Brown, T. G. Deutsch, J. A. Turner and A. M. Herring, *Energy Environ. Sci.*, 2011, **4**, 5028-5034.

[61] T. W. Kim and K. Choi, *Science*, 2014, **343**, 990-994.

[62] K. P. Bhandari, P. J. Roland, H. Mahabaduge, N. O. Haugen, C. R. Grice, S. Jeong, T.

Dykstra, J. Gao and R. J. Ellingson. *Solar Energy Mater. Solar Cell.*, 2013, **117**, 476-482.

[63] P. Mark, *Phys. Rev.*, 1965, **137**, A203-A210.

[64] J. Ebothe, *J. Appl. Phys.*, 1986, **59**, 2076-2081.

[65] B. V. Novikov, A. V. Ilinskii, K. F. Lieder and N. S. Sokolov, *Phys. Stat. Sol. B*, 1971, **48**, 473-480.

[66] C. Weber, U. Becker, R. Renner and C. Klingshirn, *Z. Phys. B-Condensed Matter*, 1988, **72**, 379-384.

[67] *Solar Hydrogen Generation: Toward a Renewable Energy Future*, ed. K. Rajeshwar, R. McConnell and S. Licht, Springer, 2008.

[68] N. Bao, L. Shen, T. Takata and K. Domen, *Chem. Mater.*, 2008, **20**, 110-117.

[69] N. Bao, L. Shen, T. Takata, K. Domen, A. Gupta, K. Yanagisawa and C. A. Grimes, *J. Phys. Chem. C*, 2007, **111**, 17527-17534.

[70] L. A. Silva, S. Y. Ryu, J. Choi, W. Choi and M. R. Hoffmann, *J. Phys. Chem. C*, 2008, **112**, 12069-12073.

[71] Y. Li, Y. Hu, S. Peng, G. Lu and S. Li, *J. Phys. Chem. C*, 2009, **113**, 9352-9358.

[72] X. Zong, H. Yan, G. Wu, G. Ma, F. Wen, L. Wang and C. Li, *J. Am.Chem. Soc.,* 2008, **130**, 7176-7177.

[73] F. A. Frame and F. Osterloh, *J. Phys. Chem. C*, 2010, **114**, 10628-10633.

[74] M. Shalom, Z. Tachan, Y. Bouhadana, H. Barad and A. Zaban, *J. Phys. Chem. Lett.*, 2011, **2**, 1998-2003.

[75] K. Wang, Z. Chen, H. Lv, H. Zhu, C. L. Hill and T. Lin, *J. Am. Chem. Soc.*, 2014, **136**, 7708-7716.

[76] J. A. del Alamo, *Nature*, 2011, **479**, 317-323.

[77] *Properties of the III-V compound semiconductors*.
http://www.semiconductors.co.uk/propiiiv5653.htm

[78] R. E. Allali, M. A. Pollack, W. D. Johnson Jr and R. L. Barns, *Appl. Phys. Lett.*, 1978, **33**, 659-661.

[79] *On Solar Hydrogen and Nanotechnology*, ed. L. Vayssieres, John Wiley & Sons (Asian), 2009.

[80] M. Lee, K. Takei, J. Zhang, R. Kapadia, M. Zheng, Y. Chen, J. Nah, T. S. Matthews, Y. Chueh, J. W. Ager and A. Javey, *Angew. Chem. Int. Ed.*, 2012, **51**, 10760-10764.

[81] P. G. P. Ang and A. F. Sommells, *J. Electrochem. Soc.*, 1984, **131**, 1462-1464.

[82] O. Khaselev, A. Bansal and J. A. Turner, *Int. J. Hydrogen Energy*, 2001, **26**, 127-132.

[83] O. Khaselev and J. A. Turner, *Science*, 1998, **280**, 425-427.

[84] *Practical Handbook of Photovoltaics: Fundamentals and Applications*, ed. V. M. Andreev, Elsevier, 2003.

[85] X. Chen and S. S. Mao, *Chem. Rev.*, 2007, **107**, 2891-2959.

[86] F. E. Osterloh, *Chem. Soc. Rev.*, 2013, **42**, 2294-2320.

[87] H. Vrubel, D. Merkia and X. Hu, *Energy Environ. Sci.*, 2012, **5**, 6136-6144.

[88] T. F. Jaramillo, K. P. Jorgensen, J. Bonde, J. H. Nielsen, S. Horch and I. Chorkendorff, *Science*, 2007, **317**, 100-102.

[89] A. Kongkanand, K. Tvrdy, K. Takechi, M. Kuno and P. V. Kamat, *J. Am. Chem. Soc.*, 2008, **130**, 4007-4015.

[90] K. Prabakar, S. Minkyu, S. Inyoung and K. Heeje. *J. Phys. D: Appl. Phys.*, 2010, **43**, 012002.

[91] R. Kasowski, *Phys. Rev. Lett.*, 1973, **30**, 1175-1178.

[92] N. Singh, G. Jabbour and U. Schwingenschlogl, *Eur. Phys. J. B.*, 2012, **85**, 392.

[93] *The Physics of Semiconductors: An Introduction Including Devices and Nanophysics*, ed. M. Grundmann, Springer, Berlin, 2006.

[94] I. Balberg and H. Pinch, *J. Magn. Magn. Mater.*, 1978, **7**, 12-15.

[95] A. Kay, I. Cesar and M. Grätzel, *J. Am. Chem. Soc.*, 2006, **128**, 15714-15721.

[96] M. Grela and A. J. Colussi, *J. Phys. Chem.*, 1996, **100**, 18214-18221.

[97] F. Formal, N. Tetreault, M. Cornuz, T. Moehl, M. Grätzel and K. Silvula, *Chem. Sci.*, 2011, **2**, 737-743.

[98] F. Formal, M. Grätzel and K. Silvula. *Adv. Funct. Mater.*, 2010, **20**, 1099-1107.

[99] S. Tanriseven and B. Corbett, *J. Appl. Phys.,* 2011, **110**, 034508.

[100] B. A. Gonfa, H. Zhao, J. Li, J. Qiu, M. Saidani, S. Zhang, R. Izquierdo, N. Wu, M. A. Khakani and D. Ma, *Solar Energy Mater. Solar Cell.*, 2014, **124**, 67-74.

[101] B. O'Regan and M. Grätzel, *Nature,* 1991, **353**, 737-740.

[102] N. Kopidakis, E. A. Schiff, N. G. Park, J. van de Lagemaat and A. J. Frank, *J. Phys. Chem. B,* 2000, **104**, 3930-3936.

[103] (*a*) J. Low, S. Cao, J. Yu and S. Wageh, *Chem. Commun.,* 2014, **50**, 10768-10777. (*b*) S.

Ida and T. Ishihara, *J. Phys. Chem. Lett.*, 2014, **5**, 2533-2542. (*c*) *Nanomaterials, Nanostructures, and Nanotechnologies*, ed. A. I. Gusev, Fizmatlit, Moscow, 2007.

[104] M. Zhou, H. B. Wu, J. Bao, L. Liang, X. W. Lou and Y. Xie, *Angew. Chem. Int. Ed.*, 2013, **52**, 8579 -8583.

[105] E. Enache-Pommer, B. Liu and E. S. Aydil. *Phys. Chem. Chem. Phys.*, 2009, **11**, 9648-9652.

[106] J. Li, M. Hoffmann, H. Shen, C. Fabrega, J. D. Prades, T. Andreu, F. Hernandez-Ramirez and S. Mathur, *J. Mater. Chem.*, 2012, **22**, 20472-20476.

[107] F. Li, J. Xu, L. Chen, B. Ni, X. Li, Z. Fu and Y. Lu, *J. Mater. Chem. A*, 2013, **1**, 225-228.

[108] X. Q. Chen, J. H. Ye, S. X. Ouyang, T. Kako, Z. S. Li and Z. G. Zou, *ACS Nano*, 2011, **5**, 4310-4318.

[109] N. Wu, J. Wang, D. N. Tafen, H. Wang, J. Zheng, J. P. Lewis, X. Liu, S. S. Leonard and A. Manivannan*, J. Am. Chem. Soc.*, 2010, **132**, 6679-6685.

[110] N. Murakami, Y. Kurihara, T. Tsubota and T. Ohno, *J. Phys. Chem. C,* 2009, **113**, 3062-3069.

[111] G. K. Mor, K. Shankar, M. Paulose and C. A. Grimes, *Nano Lett.*, 2005, **5**, 191-195.

[112] D. DeMeo, S. MacNaughton, S. Sonkusale and T. E. Vandervelde, *Electrodeposited copper oxide and zinc oxide core-shell nanowire photovoltaic cells*. In *Nanowires-Implementations and Applications*, ed. A. Hashim, InTech, 2011.

[113] O. L. Muskens, J. G. Rivas, R. E. Algra, E. P. A. M. Bakkers and A. Lagendijk, *Nano Lett.*, 2008, **8**, 2638-2642.

[114] E. Garnett and P. Yang, *Nano Lett.*, 2010, **10**, 1082-1087.

[115] L. Cao, P. Fan, A. P. Vasudev, J. S. White, Z. Yu, W. Cai, J. A. Schuller, S. Fan and A. L. Brongersma, *Nano Lett.*, 2010, **10**, 439-445.

[116] B. M. Kayes, H. A. Atwater and N. S. Lewis, *J. Appl. Phys.,* 2005, **97**, 11.

[117] Gopal K. Mor, Haripriya E. Prakasam, Oomman K. Varghese, Karthik Shankar and C. A. Grimes, *Nano Lett.*, 2007, **7**, 2356-2364

[118] Y. Lin, S. Zhou, S.W. Sheehan and D. Wang*, J. Am. Chem. Soc.,* 2011, **133**, 2398-2401.

[119] J. A. García-Calzón and M. E. Díaz-Garcí, *TrAC Trends Anal. Chem.*, 2012, **35**, 27-38.

[120] T. Baba, *Nat. Photon.*, 2008, **2**, 465-473.

[121] S. Y. Lin, J. G. Fleming, Z. Y. Li, I. El-Kady, R. Biswas and K. M. Ho, *J. Opt. Soc. Am. B,*

2003, **20**, 1538-1541.

[122] A. Tao, P. Sinsermsuksakul and P. Yang, *Nat. Nanotechnol.*, 2007, **2**, 435-440.

[123] C. Cheng, S. Karuturi, L. Liu, J. Liu, H. Li, L.T. Su, A. Tok and H. Fan, *Small*, 2012, **8**, 37-42.

[124] Z. Zhang, L. Zhang, M. N. Hedhili, H. Zhang and P. Wang, *Nano Lett.*, 2013, **13**, 14-20.

[125] *Semiconductor Nanostructures*, ed. D. Bimberg, Springer, 2008.

[126] G. Li and K. A. Gray, *Chem. Phys.*, 2007, **339**, 173-187. And reference therein.

[127] C. Colbeau-Justin and M. Kunst, D. Huguenin, *J. Mater. Sci.*, 2003, **38**, 2429-2437.

[128] T. Sumita, T. Yamaki, S. Yamamoto and A. Miyashita, *Appl. Surf. Sci.*, 2002, **200**, 21-26.

[129] A. Shiga, A. Tsujiko, S. Yae and Y. Nakato, *Bull. Chem. Soc. Japan,* 1998, **71**, 2119-2125.

[130] Q. Shen, K. Katayama, T. Sawada, M. Yamaguchi, Y. Kumagai and T. Toyoda. *Chem. Phys. Lett.*, 2006, **419**, 464-468.

[131] D. O. Scanlon, C. W. Dunnill, J. Buckeridge, S. A. Shevlin, A. J. Logsdail, S. M. Woodley, C. R. A. Catlow, M. J. Powell, R. G. Palgrave, I. P. Parkin, G. W. Watson, T. W. Keal, P. Sherwood, A. Walsh and A. A. Sokol, *Nature Mater.*, 2013, **12**, 798-801.

[132] B. Sun and P. G. Smirniotis, *Catal. Today*, 2003, **88**, 49-59.

[133] K. V. Baiju, A. Zachariah, S. Shukla, S. Biju, M. L. P. Reddy and K. G. K. Warrier, *Catal. Lett.,* 2009, **130**, 130-136.

[134] Zhang J, Xu Q, Feng Z, Li M and Li C, *Angew. Chem. Int. Ed.*, 2008, **47**, 1766-1769.

[135] D.P. Joshi and D. P. Bhatt, *IEEE Trans. Electron Devices*, 1990, **37**, 237-249.

[136] K. M. Doshchanov, *Semiconductors*, 1996, **30**, 305-310.

[137] J.J. Kelly and D.Vanmaekelbergh, *Electrochimica Acta*, 1998, **43**, 2773-2780.

[138] Z. Lai, F. Peng, H. Wang, H. Yu, S. Zhang and H. Zhao, *J. Mater. Chem. A.,* 2013, **1**, 4182-4185.

[139] Q. Wu, M. Liu, Z. Wu, Y. Li and L. Piao, *J. Phys. Chem. C,* 2012, **116**, 26800-26804.

[140] H. Yang, C. Sun, S. Qiao, J. Zou, G. Liu, S. C. Smith, H. Cheng and G. Lu, *Nature*, 2008, **453**, 638-641.

[141] Z. Zheng, X. Wang, C. Liu, K. Tan, Z. Xie and L. Zheng, *J. Mater. Chem. A.*, 2013, **1**, 12635-12640.

[142] Z. Jiao, Y. Zhang, H. Yu, G. Lu, J. Ye and Y. Bi, *Chem. Comm.*, 2013, **49**, 636-638.

[143] J. Lu, Y. Dai, H. Jin and B. Huang, *Phys. Chem. Chem. Phys.*, 2011, **13**, 18063-18068.

[144] P. A. M. Hotsenpiller, J. D. Bolt, W. E. Farneth, J. B. Lowekamp and G. S. Rohrer, *J. Phys. Chem. B*, 1998, **102**, 3216-3226.

[145] T. Ohno, K. Sarukawa and M. Matsumura, *New. J. Chem.*, 2002, **26**, 1167-1170.

[146] M. Liu, L. Piao, W. Lu, S. Ju, L. Zhao, C. Zhou, H. Li and W. Wang, *Nanoscale*, 2010, **2**, 1115-1117.

[147] *Photoelectrochemical Hydrogen Production,* ed. R. van de Krol and M. Graetzel, Springer, New York, 2012.

[148] T. Bak, J. Nowotny, M. Rekas and C.C. Sorrell. *Int. J. Hydrogen Energy*, 2002, **27**, 991-1022.

[149] *Electrochemistry of semiconductor and oxidized metal electrodes*, ed. S. R. Morrison, Plenum, New York, 1980.

[150] J. R. Bolton, A. F. Haught and R.T. Ross, *Photochemical energy storage: an analysis of limits*, in *Photochemical Conversion and Storage of Solar Energy*, ed. J.S. Connolly, Academic Press, New York, 1981.

[151] M. F. Weber and M. J. Dignam, *Int. J. Hydrogen Energy*, 1986, **11**, 225-232.

[152] R. Asashi, T. Morikawa, T. Ohwaki, K. Aoki and Y. Taga, *Science*, 2001, **293**, 269-271.

[153] E. Borgarello, J. Kiwi, M. Grätzel, E. Pellizzetti and M. Visca, *J. Am. Chem. Soc.*, 1982, **104**, 2996-3002.

[154] M. A. Henderson, J. M. White, H. Uetsuka and H. Onishi, *J. Am. Chem. Soc.*, 2003, **125**, 14974-14975.

[155] M. Anpo and M. Takeuchi, *J. Catal.*, 2003, **216**, 505-516.

[156] R. Hahn, M. Stark, M. S. Killian and P. Schmuki, *Catal. Sci. Technol.*, 2013, **3**, 1765-1770.

[157] S. Sato, *Chem. Phys. Lett.*, 1986, **123**, 126-128.

[158] S. Sakthivel and H. Kisch, *Angew. Chem. Int. Ed.*, 2003, **42**, 4908-4911.

[159] H. Irie, Y. Watanabe and K. Hashimoto, *J. Phys. Chem. B,* 2003, **107**, 5483-5486.

[160] J. Y. Lee, J. Park and J. H. Cho. *Appl. Phys. Lett.*, 2005, **87**, 011904.

[161] M. Batzil, E. H. Morales and U. Diebold, *Phys. Rev. Lett.*, 2006, **96**, 026103.

[162] J. Wang, D. Tafen, J. Lewis, Z. Hong, A. Manivannan, M. Zhi, M. Li and N. Wu, *J. Am. Chem. Soc.*, 2009, **131**, 12290-12297.

[163] D. Tafen, J. Wang, N. Q. Wu and J. P. Lewis, *Appl. Phys. Lett.,* 2009, **94**, 093101.

[164] T. Miyagi, M. Kamei, I. Sakaguchi, T. Mitsuhashi and A. Yamazaki*, Jpn. J. Appl. Phys.*,

2004, **43**,775-776.

[165] H. P. Maruska and A. K. Ghosh, *Solar Energy Mater.,* 1979, **1**, 237-247.

[166] P. Salvador, *Solar Energy Mater.,* 1982, **6**, 241-250.

[167] X. Y. Meng, G. W. Qin, S. Li, X. H. Wen, Y. P. Ren, W. L. Pei and L. Zuo, *Appl. Phys. Lett.*, 2011, **98**, 112104,

[168] W. Choi, A. Termin and M. R. Hoffman, *J. Phys. Chem.*, 1994, **98**, 13669-13679.

[169] X. Chen, L. Lu, P. Y. Yu and S. S. Mao, *Science*, 2011, **331**, 746-750.

[170] Y. H. Hu, *Angew. Chem. Int. Ed.*, 2012, **51**, 12410-12412.

[171] G. Wang, H. Wang, Y. Ling, Y. Tang, X. Yang, R. C. Fitzmorris, C. Wang, J. Z. Zhang and Y. Li, *Nano Lett.*, 2011, **11**, 3026-3033.

[172] C. Yang, Z. Wang, T. Lin, H. Yin, X. Lv, D. Wan, T. Xu, C. Zheng, J. Lin, F. Huang, X. Xie and M. Jiang, *J. Am. Chem. Soc.*, 2013, **135**, 17831-17838.

[173] Z. Wang, C. Yang, T. Lin, H. Yin, P. Chen, D. Wan, F. Xu, F. Huang, J. Lin, X. Xie and M. Jiang, *Energy Environ. Sci.*, 2013, **6**, 3007-3014.

[174] T. Lin, C. Yang, Z. Wang, H. Yin, X. Lv, F. Huang, J. Lin, X. Xie and M. Jiang, *Energy Environ. Sci.*, 2014, **7**, 967-972.

[175] T. Xia and X. Chen, *J. Mater. Chem. A*, 2013, **1**, 2983-2989.

[176] H. Cui, W. Zhao, C. Yang, H. Yin, T. Lin, Y. Shan, Y. Xie and F. Huang, *J. Mater. Chem. A*, 2014, **2**, 8612-8616.

[177] N. Liu, C. Schneider, D. Freitag, M. Hartmann, U. Venkatesan, J. Mueller, E. Spiecker and P. Schmuki, *Nano Lett.*, 2014, **14**, 3309-3313.

[178] M. Li, J. Zhang, W. Dang, S. K. Cushing, D. Guo, N. Q. Wu and P. Yin, *Phys. Chem. Chem. Phys.*, 2013, **15**, 16220-16226.

[179] F. Meng, Z. Hong, J. Arndt, M. Li, M. Zhi, F. Yang and N. Wu, *Nano Res.*, 2012, **5**, 213-221.

[180] F. Meng, J. Li, Z. Hong, M. Zhi, A. Sakla, C. Xiang and N. Wu, *Catal. Today*, 2013, **199**, 48-52.

[181] S. H. Wei and A. Zunger, *Phys. Rev. B*, 1988, **37**, 8958-8981.

[182] K. Maeda, T. Takata, M. Hara, N. Saito, Y. Inoue, H. Kobayashi and K. Domen, *J. Am. Chem. Soc.*, 2005, **127**, 8286-8287.

[183]Y. Lee, H. Terashima, Y. Shimodaira, K. Teramura, M. Hara, H. Kobayashi, K. Domen and

M. Yashima, *J. Phys. Chem. C,* 2007, **111**, 1042-1048.

[184] M. Kitano and M. Hara, *J. Mater. Chem.*, 2010, **20**, 627-641.

[185] S. X. Ouyang and J. H. Ye, *J. Am. Chem. Soc.*, 2011, **133**, 7757-7763.

[186] D. F. Wang, T. Kako and J. H. Ye, *J. Phys. Chem. C*, 2009, **113**, 3785-3792.

[187] W. F. Yao and J. H. Ye, *J. Phys. Chem. B*, 2006, **110**, 11188-11195.

[188] S. Linic, P. Christopher and D. B. Ingram, *Nature Mater.*, 2011, **10**, 911-921.

[189] S. K. Cushing and N. Wu, *Interface*, 2013, **2**, 63-67.

[190] H. A. Atwater and A. Polman, *Nature Mater.*, 2010, **9**, 205-213.

[191] C. Clavero, *Nature Photonics*, 2014, **8**, 95-103.

[192] S. C. Warren and E. Thimsen, *Energy Environ. Sci.*, 2012, **5**, 5133.

[193] J. Li, S. K. Cushing, P. Zheng, F. Meng, D. Chu and N. Wu, *Nature Commun.*, 2013, **4**, 2651.

[194] Y. Tian and T. Tatsuma, *Chem. Commun.*, 2004, 1810-1811.

[195] Y. Tian and T. Tatsuma, *J. Am. Chem. Soc.*, 2005, **127**, 7632-7637.

[196] S. K. Cushing, J. T. Li, F. Meng, T. R. Senty, S. Suri, M. Zhi, M. Li, A. D. Bristow and N. Wu, *J. Am. Chem. Soc.*, 2012, **134**, 15033-15041.

[197] J. Mertz, *J. Opt. Soc. Am. B*, 2000, **17,** 1906-1913.

[198] *Surface Plasmon on Smooth and Rough Surfaces and on Gratings*, ed. H. Raether, Springer, 1988.

[199] H. Gao, H. Jeong and P. Yang, *ACS Nano*, 2012, **6**, 234-240.

[200] H. Dotan, O. Kfir, E. Sharlin, O. Blank, M. Gross, I. Dumchin, G. Ankonina and A. Rothschild, *Nature Mater.*, 2013, **12**, 158-164.

[201] M. W. Knight, H. Sobhani, P. Nordlander and N. J. Halas, *Science*, 2011, **332**, 702-704.

[202] F. Wang and N. A. Melosh, *Nano Lett.*, 2011, **11**, 5426-5430.

[203] Y. Nishijima,K. Ueno, Y. Kotake, K. Murakoshi, H. Inoue and H. Misawa, *J. Phys. Chem. Lett.*, 2012, **3**, 1248-1252.

[204] M. W. Knight, Y. Wang, A. S. Urban, A. Sobhani, B. Zheng, P. Nordlander and N. J. Halas, *Nano Lett.*, 2013, **13**, 1687-1692.

[205] S. Mubeen, J. Lee, N. Singh, S. Kraemer, G. D. Stucky and M. Moskovits, *Nature Nanotechnol.*, 2013, **8**, 247-251.

[206] S. Mubeen, C. Hernandez-Sosa, D. Moses, J. Lee and M. Moskovits, *Nano Lett.*, 2011, **11**,

5548-5552.

[207] J. Li, S. K. Cushing, J. Bright, F. Meng, T. Senty, P. Zheng, A. Bristow and N. Wu, *ACS Catal.*, 2013, **3**, 47-51.

[208] K. Wu, W. E. Rodríguez-Córdoba, Y. Yang and T. Lian, *Nano Lett.*, 2013, **13**, 5255-5263.

[209] T. P. White and K. R. Catchpole, *App. Phys. Lett.*, 2012, **101**, 073905.

[210] A. O. Govorova, H.Zhang, H. V. Demirb and Y. K. Gunkod, *Nano Today*, 2014, **9**, 85-101.

[211] Y. Pu, G. Wang, K. Chang, Y. Ling, Y. Lin, B. Fitzmorris, C. Liu, X. Lu, Y. Tong, J. Zhang, Y, Hsu and Y. Li, *Nano Lett.*, 2013, **13**, 3817-3823.

[212] K. Kimura, S. Naya, Y. Jin-nouchi and H. Tada, *J. Phys. Chem. C*, 2012, **116**, 7111-7117.

[213] A. Furube, L. Du, K. Hara, R. Katoh and M. Tachiya, *J. Am. Chem. Soc.*, 2007, **129**, 14852-14853.

[214] H. Inouye, K. Tanaka, I. Tanahashi and K. Hirao, *Phys. Rev. B*, 1998, **57**, 11334-11340.

[215] M. K. Kumar, S. Krishnamoorthy, L. K. Tan, S. Y. Chian, S. Tripathy and H. Gao, *ACS Catal.*, 2011, **1**, 300-308.

[216] I. Thomann, B. A. Pinaud, Z. Chen, B. M. Clemens, T. F. Jaramillo and M. L. Brongersma, *Nano Lett.*, 2011, **11**, 3440-3446.

[217] K. Awazu, M. Fujimaki, C. Rockstuhl, J. Tominaga, H. Wurakami, Y. Ohki, N. Yoshida and T. Watanabe, *J. Am. Chem. Soc.*, 2008, **130**, 1676-1680.

[218] T. Torimoto, H. Horibe, T. Kameyama, K. Okazaki, S. Ikeda, M. Matsumura, A. Ishikawa and H. Ishihara, *J. Phys. Chem. Lett.*, 2011, **2**, 2057-2062.

[219] J. Zhou, F. Ren, S. Zhang, W. Wu, X. Xiao, Y. Liu and C. Jiang, *J. Mater. Chem. A*, 2013, **1**, 13128-13138.

[220] J. Xu, X. Xiao, A. Stepanov, F. Ren, W. Wu, G. Cai, S. Zhang, Z. Dai, F. Mei and C. Jiang, *Nanoscale Res. Lett.*, 2013, **8**, 73.

[221] K. Aydin, V. E. Ferry, R. M. Briggs and H. A. Atwater, *Nature Commun*., 2011, **2**, 517,

[222] J.-H. Yana, Y.-R. Zhua, Y.-G. Tanga and S. Q. Zhenga. *J. Alloys Comp.*, 2009, **472**, 429-433.

[223] J. Zhang, J. H. Bang, C. Tang and P. V. Kamat, *ACS Nano,* 2010, **4**, 387-395.

[224] N. R. D'Amico, G. Cantele and D. Ninno, *Appl. Phys. Lett.,* 2012, **101**, 141606.

[225] J. S. Jang, H. G. Kim and J. S. Lee, *Catal. Today*, 2012, **185**, 270-277.

[226] Y. Lin, Y. Xu, M. T. Mayer, Z. I. Simpson, G. McMahon, S. Zhou and D. Wang, *J. Am.*

Chem. Soc., 2012, **134**, 5508-5511.

[227] M. T. Mayer, Y. Lin, G. Yuan and D. Wang, *Acc. Chem. Res.*, 2013, **46**, 1558-1566.

[228] F. Meng, J. Li, S. K. Cushing, M. Zhi and N. Wu, *J. Am. Chem. Soc.*, 2013, **135**, 10286-10289.

[229] M. Wang, L. Sun, Z. Lin, J. Cai, K. Xie and C. Lin, *Energy Environ. Sci.*, 2013, **6**, 1211-1220.

[230] T. Tsai, S. Chang, T. Hsueh, H. Hsueh, W. Weng, C. Hsu and B. Dai, *Nanoscale Res. Lett.*, 2011, **6**, 575.

[231] H. G. Kim, P. H. Borse, W. Choi and J. S. Lee, *Angew. Chem. Int. Ed.*, 2005, **117**, 4661-4665.

[232] H. G. Kim, P. H. Borse, J. S. Jang, E. D. Jeong, O. S. Jung, Y. J. Suh and J. S. Lee, *Chem. Commun.*, 2009, **39**, 5889-5991.

[233] N. Serpone, E. Borgarelo and M. Grätzel, *J. Chem. Soc. Chem. Commun.,* 1984, 342-344.

[234] J. Yoshimura, A. Kudo A. Tanaka, K. Domen, K. Maruya and T. Onishi, *Chem. Phys. Lett.,* 1988, **147**, 401-404.

[235] H. Gerischer and M. Luebke, *J. Electroanal. Chem.*, 1986, **204**, 225-227.

[236] S. Kohtani, A. Kudo and T. Sakata, *Chem. Phys. Lett.,* 1993, **206**, 166-170.

[237] D. Wang, H. Zhao, N. Wu, M. Khahani and D. Ma, *J. Phys. Chem. Lett.*, 2010, **1**, 1030-1035.

[238] H. Kim, J. Kim, W. Kim and W. Choi, *J. Phys. Chem. C*, 2011, **115**, 9797-9805.

[239] R. M. Navarro, F. del Valle and J. L. G. Flerro. *Int. J. Hydrogen Energy*, 2008, **33**, 4265-4273.

[240] Y. Qu and X. Duan, *Chem. Soc. Rev.*, 2013, **42**, 2568-2580.

[241] G. Konstantatos, I. Howard, A. Fischer, S. Hoogland, J. Cliford, E. Klem, L. Levina and E. H. Sargent, *Nature*, 2006, **442**, 180-183.

[242] S. A. Mcdonald, G. K. Konstantatos, S. Zhang, P. W. Cyr, E. J. D. Klem, L. Levina and E. H. Sargent, *Nat. Mater.*, 2005, **4**, 138-142.

[243] D. M. N. M. Dissanayake, T. Lutz, R. J. Curry and S. R. P. Silva, *Appl. Phys. Lett.,* 2008, **93**, 043501.

[244] J. Linnros, *J. Appl. Phys.*, 1998, **84**, 275-283.

[245] J. Linnros, *J. Appl. Phys.,* 1998, **84**, 284-291.

[246] P. Landsberg, *Appl. Phys. Lett.,* 1987, **50**, 745-747.

[247] A. Paracchino, V. Laporte, K. Sivula, M. Grätzel and E. Thimsen, *Nature Mater.*, 2011, **10**, 456-461.

[248] M. T. Mayer, C. Du and D. Wang, *J. Am. Chem. Soc.,* 2012, **134**, 12406-12409.

[249] Y. Hwang, A. Boukai and P. Yang, *Nano Lett.,* 2009, **9**, 410-415.

[250] Y. Yu, J. Yu, J. G. Yu, Y. Kwok, Y. Che, J. Zhao, L. Ding, W. Ge and P. Wong, *Appl. Catal. A*, 2005, **289**, 186-196.

[251] A. Kongkanand, R. M. Domínguez and P. V. Kamat, *Nano Lett.,* 2007, **7**, 676-680.

[252] K. Woan, G. Pyrgiotakis and W. Sigmund, *Adv. Mater.,* 2009, **21**, 2233-2239.

[253] G. Williams, B. Seger and P. V. Kamat, *ACS Nano*, 2008, **2**, 1487-1491.

[254] H. Zhang, X. J. Lv, Y. M. Li, Y. Wang and J. H. Li, *ACS Nano*, 2010, **4**, 380-386.

[255] Q. J. Xiang, J. G. Yu and M. Jaroniec, *Chem. Soc. Rev.,* 2012, **41**, 782-796.

[256] Y. H. Ng, A. Iwase, A. Kudo and R. Amal, *J. Phys. Chem. Lett.*, 2010, **1**, 2607-2612.

[257] X. Y. Zhang, H. P. Li, X. L. Cui and Y. H. Lin, *J. Mater. Chem.,* 2010, **20**, 2801-2806.

[258] S. Stankovich, D. A. Dikin, G. H. B. Dommett, K. M. Kohlhaas, E. J. Zimney, E. A. Stach, R. D. Piner, S. T. Nguyen and R. S. Ruoff, *Nature*, 2006, **442**, 282-286.

[259] F. Meng, J. Li, S. K. Cushing, J. Bright, M. Zhi, J. Rowley, Z. Hong, A. Manivannan, A. D. Bristow and N. Q. Wu, *ACS Catal.*, 2013, **3**, 746-751.

[260] J Sun, H. Zhang, L. Hong Guo and L. Zhao, *ACS Appl. Mater. Interfaces,* 2013, **5**, 13035-13041.

[261] Y. Hou, F. Zuo, A. Dagg and P. Feng, *Nano Lett.*, 2012, **12**, 6464-6473.

[262] J. Brillet, J. Yum, M. Cornuz, T. Hisatomi, R. Solarska, J. Augustynski, M. Graetzel and K. Sivula, *Nature Photonics*, 2012, **6**, 824-828.

[263] S. Y. Reece, J. A. Hamel, K. Sung, T. D. Jarvi, A. J. Esswein, J. J. H. Pijpers and D. G. Nocera, *Science*, 2011, 334, 645-648.

[264] Y. Tachibana, L. Vayssieres and J. R. Durrant, *Nature Photonics*, 2012, **6**, 511-518.

[265] K. Maeda and K. Domen, *J. Phys. Chem. Lett.*, 2010, **1**, 2655-2661.

[266] K. Maeda, *ACS Catal.,* 2013, **3**, 1486-1503.

[267] A. Kudo, *MRS Bulletin*, 2011, **36**, 32-38.

[268] H. Kato, M. Hori, R. Konta, Y. Shimodaira and A. Kudo, *Chem. Lett.*, 2004, **33**, 1348-1349.

[269] M. Higashi, R. Abe, K. Teramura, T. Takata, B. Ohtani and K. Domen, *Chem. Phys. Lett.*,

2008, **452**, 120-123.

[270] M. Higashi, R. Abe, T. Takata and K. Domen, *Chem. Mater.*, 2009, **21**, 1543-1549.

[271] K. Maeda, R. Abe and K. Domen, *J. Phys. Chem. C,* 2011, **115**, 3057-3064.

[272] R. Abe, M. Higashi and K. Domen, *ChemSusChem*, 2011, **4**, 228-237.

[273] M. Higashi, R. Abe, A. Ishikawa, T. Takata, B. Ohtani and K. Domen, *Chem. Lett.*, 2008, **37**, 138-139.

[274] Y. Sasaki, H. Kato and A. Kudo, *J. Am. Chem. Soc.*, 2013, **135**, 5441-5449.

[275] Y. Sasaki, H. Nemoto, K. Saito and A. Kudo, *J. Phys. Chem. C*, 2009, **113**, 17536-17542.

[276] S. S. K. Ma, K. Maeda, T. Hisatomi, M.Tabata and K. Domen, *Chem.-Eur. J.*, 2013, **19**, 7480-7486.

[277] R. Abe, K. Sayama, K. Domen and H. Arakawa, *Chem. Phys. Lett.*, 2001, **344**, 339-344.

[278] K. Maeda, D. Lu and K. Domen, *ACS Catal.,* 2013, **4**, 1013-1021.

[279] A. Iwase, Y. H. Ng, Y. Ishiguro, A. Kudo and R. Amal, *J. Am. Chem. Soc.*, 2011, **133**, 11054-11057.

[280] H. Tada, T. Mitsui, T. Kiyonaga, T. Akita and K. Tanaka, *Nature Mater.,* 2006, **5**, 782-786.

[281] H. J. Yun, H. Lee, N. D. Kim, D. M. Lee, S. Yu and J. Yi, *ACS Nano*, 2011, **5**, 4084-4090.

[282] J. Yang, D. Wang, H. Han and C. Li, *Acc. Chem. Res.*, 2013, **46**, 1900-1909.

[283] I. Man, H-Y. Su, F. Vallejo, H. Hansen, J. Martinez, N. Inoglu, J. Kitchin, T. Jaramillo, J. Nørskov and J. Rossmeisl, *ChemCatChem*, 2011, **3**, 1159-1165;

[284] C. G. Morales-Guio, L.-A. Stern and X. Hu, *Chem. Soc. Rev.,* 2014, **43**, 6555-6569.

[285] S. Trasatti, *Electrochim. Acta.*, 1984, **29**, 1503-1512.

[286] E. Fabbri, A. Habereder, K. Waltar, R. Ktz and T. J. Schmidt, *Catal. Sci. Technol.*, 2014, DOI: 10.1039/C4CY00669K.

[287] S. C. Riha, B. M. Klahr, E. C. Tyo, S. Seifert, S. Vajda, M. J. Pellin, T.W. Hamann and A. B. F. Martinson, *ACS Nano*, 2013, **7**, 2396-2405.

[288] Li. Xi, P. D. Tran, S. Y. Chiam, P. S. Bassi, W. F. Mak, H. K. Mulmudi , S. K. Batabyal, J. Barber, J. S. C. Loo and L. H. Wong, *J. Phys. Chem. C*, 2012, **116**, 13884-13889.

[289] M. W. Kanan and D. G. Nocera, *Science*, 2008, **321**, 1072-1075.

[290] D. K. Zhong, S. Choi and D. R. Gamelin, *J. Am. Chem. Soc.*, 2011, **133**, 18370-18377.

[291] B. Klahr, S. Gimenez, F. Fabregat-Santiago, J. Bisquert and T. W. Hamann, *J. Am. Chem. Soc.*, 2012, **134**, 16693-16700.

[292] E. M. P. Steinmiller and K. S. Choi, *Proc. Natl. Acad. Sci. U. S. A.*, 2009, **106**, 20633-20636.

[293] M. Bledowski, L. Wang, A. Ramakrishnan, A. Bétard, O. Khavryuchenko and R. Beranek, *ChemphysChem*, 2012, **13**, 3018-3024.

[294] Q. Liu, Q. Chen, J. Bai, J. Li, J. H. Li and B. Zhou, *J. Solid. State Electrochem.*, 2014, **18**, 157-161.

[295] W. D. Chemelewski, H. Lee, J. Lin, A. J. Bard and C. B. Mullins, *J. Am. Chem. Soc.*, 2014, **136**, 2843-2850.

[296] L. Trotochaud, S. L. Young, J. K. Ranney and S. W. Boettcher, *J. Am. Chem. Soc.*, 2014, **136**, 6744-6753.

[297] S. Trasatti, *J. Electroanal. Chem.*, 1972, **39**, 163-184.

[298] P. Kamat, *J. Phys. Chem. Lett.*, 2012, **3**, 663-672.

[299] K. Maeda, K. Teramura, D. Lu, N. Saito, Y. Inoue and K. Domen, *Angew. Chem. Int. Ed.,* 2006, **45**, 7970-7973.

[300] A. B. Laursen, S. Kegnas, S. Dahl and I. Chorkendorff, Energy *Environ. Sci.*, 2012, **5**, 5577-5591.

[301] Y. G. Li, H. L. Wang, L. M. Xie, Y. Y. Liang, G. S. Hong and H. J. Dai, *J. Am. Chem. Soc.*, 2011, **133**, 7296-7299.

[302] J. K. Lee, W. Lee, T. J. Yoon, G. S. Park and J. H. Choy, *J. Mater. Chem.*, 2002, **12**, 614-618.

[303] T. F. Jaramillo, K. P. Jorgensen, J. Bond, J. H. Nielsen, S. Horch and I. Chorkendorff, *Science*, 2007, **317**, 1284-1287.

[304] Y. Hou, B. L. Arams, P. Vesborg, M. Bjoerketun, K. Herbst, L. Bech, A. Setti, C. Damsgaard, T. Pedersen, O. Hansen, J. Rossmeisl, S. Dahl, J. K. Norskov and I. Chorkendorff, *Nature Mater.*, 2011, **10**, 434-438.

[305] F. A. Frame and F. Osterloh, *J. Phys. Chem. C*, 2010, **114**, 10628-10633.

[306] X. Zong, H. Yan, G. Wu, G. Ma, F. Wen, L. Wang and C. Li, *J. Am. Chem. Soc.*, 2008, **130**, 7176-7177.

[307] B. Hinnemann, P. Moses, J. Bonde, K. Jorgensen, J. Nielsen, S. Horch, I. Chorkendorff and J. Norskov, *J. Am. Chem. Soc.*, 2005, **127**, 5308-5309.

[308] Y. Hou, Z. Wen, S. Cui, X. Guo and J. Chen, *Adv. Mater.*, 2013, **25**, 6291-6297.

[309] Y. Yan, B. Xia, Z. Xu and X. Wang, *ACS Catal.*, 2014, **4**, 1693-1705

[310] D. Voiry, H. Yamaguchi, J. Li, R. Silva, D. Alves, T. Fujita, M. Chen, T. Asefa, V. Shenoy, G. Eda and M. Chhowalla, *Nature Mater.*, 2013, **12**, 850-855.

[311] W. Zhang, Y. Wang, Z. Wang, Z. Zhong and R. Xu, *Chem. Commun.*, 2010, **46**, 7631-7633.